MATERIAL CHARACTERIZATION OF ALCOHOL-WATER MIXTURES FOR THE NUMERICAL SIMULATION OF HEAT TRANSFER IN MICRO-CHANNELS

A THESIS SUBMITTED TO THE GRADUATE DIVISION OF THE
UNIVERSITY OF HAWAIʻI AT MĀNOA IN PARTIAL FULFILLMENT
OF THE REQUIREMENTS FOR THE DEGREE OF

MASTER OF SCIENCE
IN
MECHANICAL ENGINEERING

AUGUST 2012

By
Matthew Asada

Thesis Committee:

Weilin Qu, Chairperson
Beei-Huan Chao
Marcelo Kobayashi

Acknowledgments

This study was made possible through the support of the ACS Petroleum Research Fund (PRF # 47738-G6) and the National Science Foundation (CBET-1034242). The author would like to thank his advisor Professor Weilin Qu for his guidance and support throughout his academic career. Also, thanks to Professors Chao and Kobayashi for their role as mentors and members of the thesis committee. Lastly, thanks to Chun Ka Kwok and Jonathan Mita for their support with experimentation and numerical simulation.

Abstract

In this study, improved material property correlations are developed for the pure substances methanol and ethanol as well as mixtures of alcohol and water. Previously, a linear, ideal mixing rule was used for the material properties of a binary methanol/water mixture. This approach leads to error in property values of up to 50% for certain properties. Improved correlations have reduced errors in mixture property predictions to 3-8%. These new correlations are then used in the three-dimensional numerical simulation of single-phase heat transfer characteristics of binary methanol-water mixtures in a micro-channel heat sink which contains an array of 22 micro-channels with 240μm x 630μm cross-section. Pure water, pure methanol, and five methanol-water mixtures with methanol molar fraction of 16%, 36%, 50%, 63% and 82% were simulated. Numerical results are then validated against experimental data previously obtained by Chun Ka Kwok. Key parametric trends are identified and discussed. Numerical predictions and experimental data are in good agreement with a mean absolute error (MAE) of 0.87%.

Table of Contents

List of Figures

List of Tables

Nomenclature

A_t	Area of Top Platform
c_p	Specific Heat Capacity
G	Mass Velocity
h	Enthalpy
k	Thermal Conductivity
M	Molecular Weight
$\dot{m}$	Mass Flow Rate
MAE	Mean Absolute Error
P	Pressure
Psat	Saturation Pressure
Δp	Pressure Drop
T	Temperature
T_{tc}	Temperature at Thermocouple
w	Mass Fraction
x	Molar Fraction

Greek Symbols

α	Lobe Correlation Coefficient
μ	Dynamic Viscosity
ρ	Density
σ	Surface Tension
Φ, ϕ	Volume Fraction
φ	Interaction Parameter

Subscripts

aw	Air Water Mixture
c	Organic Compound
f	Fluid Phase
g	Vapor phase
H_2O	Water
i	Pure Component i
ij	Position i, j
in	Inlet
j	Pure Component j
m	Mixture
org	Organic Compound
out	Outlet
tot	Total of Mixture Components

Chapter 1: Introduction

1.1 Background

The current trend of multi-core processors is the result of cooling techniques not being able to keep up with heat generated by single core processors. The multi-core solution employs more processing units at lower clock speeds in order to distribute the thermal load over a wider area, but this is not ideal for computational speed. As seen in the field of high-performance computing, speedup values using multiple processors begin to asymptote out according to Amdahl's Law. The reason for this asymptotic trend is because more resources need to be spent to manage the communications between each processor as more units are added to a given system.

Even with a multi-core processor design, heat sinks using air are reaching their effective limit, new cooling techniques able to dissipate large heat fluxes are essential to further increase processing speeds. Liquid-cooled miniature heat sinks incorporating micro-scale flow channels are being studied extensively within the past two decades for their high heat flux cooling capabilities [1-6].

1.2 Literature Review

Since its introduction in 1981 by Tuckerman and Pease [1], the concept of a micro-channel heat sink has been heavily researched over the past three decades [2-6]. Nearly all the previous studies on micro-channel heat sinks adopted pure (single-component) liquids as working fluid [7-10]. These studies focus on developing predictive tools for the heat and mass transfer of a working fluid through micro-channels through experimentation. The working fluid for these studies is a pure fluid, either water or refrigerant. While some studies employed refrigerant mixtures [11-13], their behavior differs greatly from aqueous mixtures of alcohols.

Recently a study performed by Chun Ka Kwok [17] has found that better coolant performance may be achieved by using liquid mixtures; for example, mixture coolants could be easily functionalized for specific heat sink applications by selecting suitable combinations of pure components and then adjusting the mixture compositions. Methanol-water mixtures take advantage of both the high heat transfer capability of water and lower boiling point of methanol [17].

While NIST provides much information about the mixture properties of water and alcohol [14-16], it is unable to calculate the transport properties of viscosity and thermal conductivity of aqueous mixtures for unspecified reasons. Experimental studies have been performed to determine the liquid mixture viscosity of methanol-water [23] and ethanol-water [31] mixtures. However, for vapor mixture viscosity and thermal conductivity, there was no experimental data available. Empirical mixing rules for general aqueous mixtures of polar compounds were used [20, 28].

1.3 Research Objectives

This study was motivated by the lack of knowledge on thermal/fluid transport processes associated with liquid mixtures in micro-channels; the main goal being to increase the accuracy of the numerical simulation of a two-phase micro-fluidic system using an alcohol water mixture. For this purpose, a comprehensive program for the calculation of thermodynamic and transport properties of methanol-water and ethanol-water was developed. Through the use of improved property correlations, better predictions of the performance of a given system can be made. New property correlations based on accurate thermodynamic and transport property information will be developed for use in three-dimensional numerical simulations of heat transfer in a micro-channel heat sink. Numerical predictions for a single phase system using methanol-water mixtures will then be validated against experimental results obtained in a previous study conducted by Chun Ka Kwok.

Chapter 2 shows the improved property correlations that have been developed for a binary methanol-water mixture. Chapter 3 includes property correlations for ethanol-water mixtures. Chapter 4 presents and discusses the experimental and numerical results obtained thus far. Finally, chapter 5 summarizes the effectiveness of the new property correlations that was verified by comparing the numerical and experimental data.

Chapter 2: Thermo-Physical and Transport Properties of Methanol-Water Mixtures

The thermodynamic and transport properties of pure methanol and water were obtained using the REFPROP 9.0 database available from NIST [14]. The database uses the most accurate equations available worldwide [15]; uncertainties of 0.5% are highest reported error values but are generally much lower. Typically, equations of state explicit in excess Helmholtz energy are used by the REFPROP program to calculate material properties [16]. The source of the equations of state for each substance will be given in the appropriate section. Due to the complexity of the state equations, computational times can be long. In order to reduce computational time during simulations, 4th order polynomial curves were fitted to the REFPROP output. All properties are in SI units. The input temperature is in degrees Celsius to remain consistent with the convention used in the study performed by Chun Ka Kwok [17].

2.1 Pure Water

Due to the maturity of the state equations for water [18], the properties of water derived in the previous study [17] agreed very well with the NIST output with the exception of c_{pg} and k_g. The polynomial correlations for saturated water vapor specific heat and thermal conductivity were redone and the results along with the MAE values are presented in Table 2.1 and Table 2.2. Data was taken for a range of temperatures of 0-200°C and errors were averaged over 20,000 data points to obtain the MAE values. The remaining pure water properties can be found in Appendix A.

Table 2.1: Polynomial Coefficients for Vapor Phase Water

	$f(T)=a1*T^4+a2*T^3+a3*T^2+a4*T+a5$				
$c_{pg}(T)$	a1	a2	a3	a4	a5
T<65	3.987×10^{-7}	4.058×10^{-5}	1.084×10^{-3}	1.047	1.884×10^{3}
T≥65	-2.130×10^{-7}	2.248×10^{-4}	-1.555×10^{-2}	1.213	1.911×10^{3}
$k_g(T)$					
T<65	2.964×10^{-12}	-2.450×10^{-10}	2.724×10^{-7}	5.253×10^{-5}	1.707×10^{-2}
T≥65	7.730×10^{-12}	-1.879×10^{-10}	3.820×10^{-7}	3.712×10^{-5}	1.768×10^{-2}

Table 2.2: MAE of the Vapor Phase Water Polynomial Correlations

Property	MAE (%)
$c_{pg}(T)$	0.00422
$k_g(T)$	0.16701

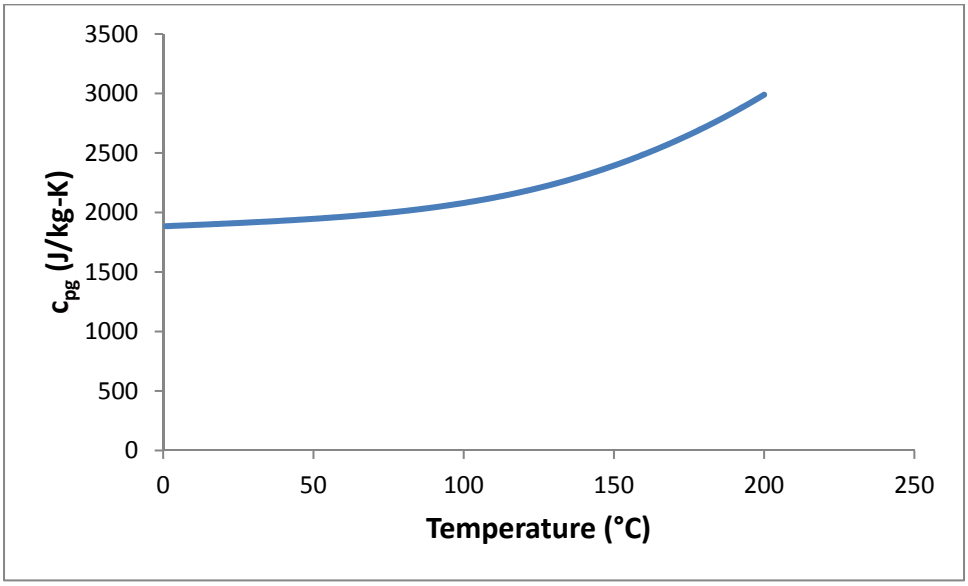

Figure 2.1: Saturated Water Vapor Specific Heat Capacity

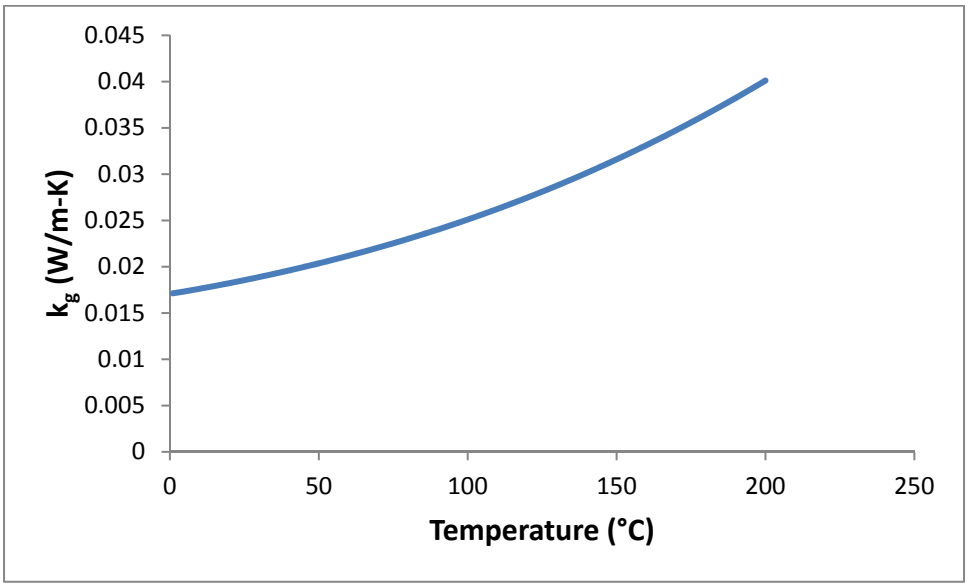

Figure 2.2: Saturated Water Vapor Thermal Conductivity

2.2 Pure Methanol

Saturated liquid properties of methanol were calculated using the equations of state found in the REFPROP program [19]. The result was then correlated using polynomials as a function of temperature for use in numerical simulation. A summary of the polynomial coefficients are presented in Table 2.9. All properties are in SI units. The polynomial correlations and the NIST outputs were compared over a range of 0-200°C; the error was calculated for 20,000 data points and averaged. A summary of the MAE values of the liquid properties are presented in Table 2.10.

2.2.1 Liquid Phase

Table 2.3: Polynomial Coefficients for Liquid Density and Specific Heat Capacity

	$f(T)=a1*T^4+a2*T^3+a3*T^2+a4*T+a5$				
$\rho(T)$	a1	a2	a3	a4	a5
T<65	-2.086×10^{-8}	-5.043×10^{-6}	2.214×10^{-4}	-0.9382	809.646
T≥65	-1.628×10^{-7}	5.755×10^{-5}	-9.929×10^{-3}	-0.2220	791.160
$c_p(T)$					
T<65	-1.474×10^{-7}	-2.639×10^{-6}	0.03263	4.532	2401.06
T≥65	9.634×10^{-6}	-4.203×10^{-3}	0.7156	-44.25	3678.00

Table 2.4: MAE Values for Liquid Density and Specific Heat Capacity

Property	MAE (%)
$\rho(T)$	0.00600
$c_p(T)$	0.08419

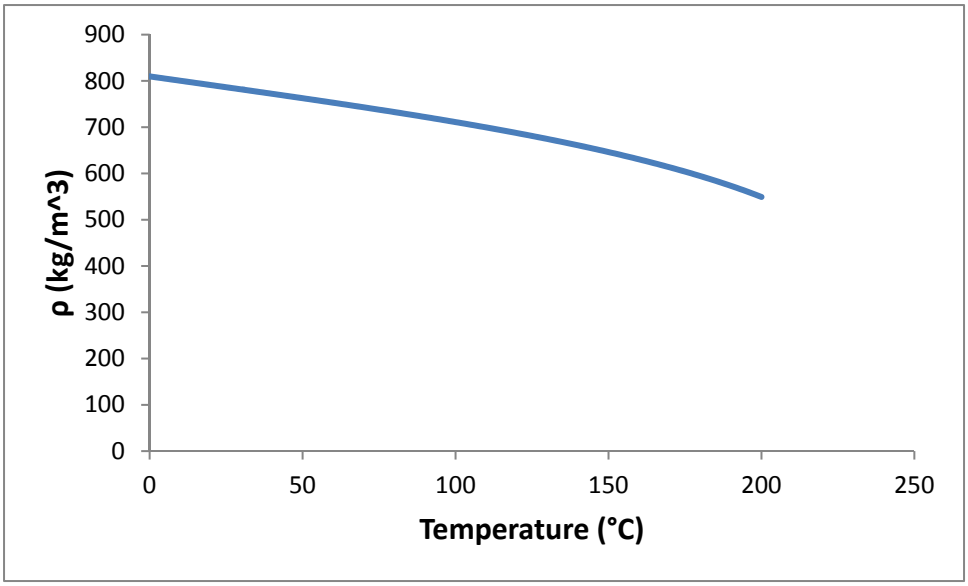

Figure 2.3: Methanol Liquid Density

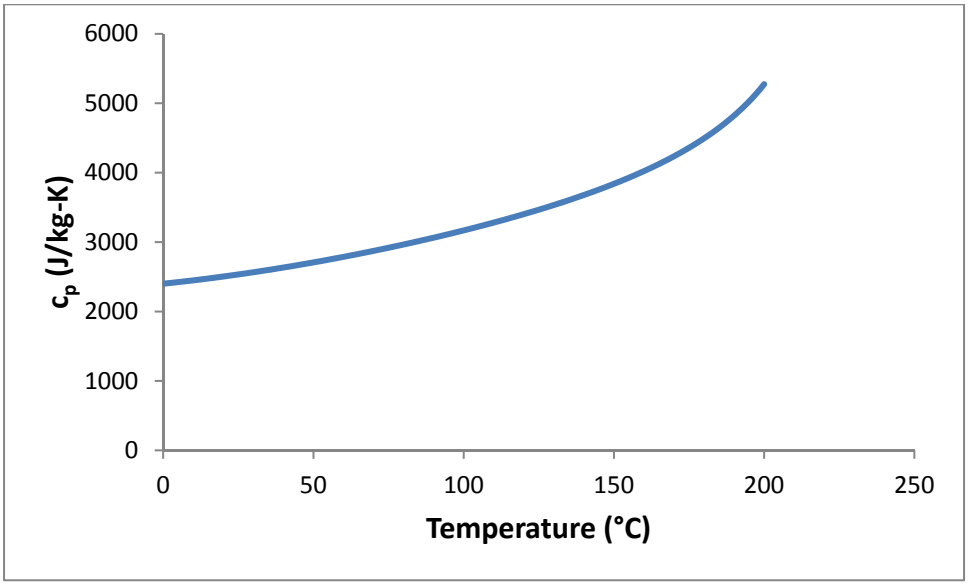

Figure 2.4: Methanol Liquid Specific Heat Capacity

Table 2.5: Polynomial Coefficients for Liquid Thermal Conductivity and Viscosity

	$f(T)=a1*T^4+a2*T^3+a3*T^2+a4*T+a5$				
k(T)	a1	a2	a3	a4	a5
T<65	$1.051x10^{-11}$	$-7.967x10^{-9}$	$1.833x10^{-6}$	$-3.873x10^{-4}$	0.2094
T≥65	$2.505x10^{-11}$	$-1.468x10^{-8}$	$3.005x10^{-6}$	$-4.757x10^{-4}$	0.2118
μ(T)					
T<65	$4.667x10^{-12}$	$-1.218x10^{-9}$	$1.564x10^{-7}$	$-1.371x10^{-5}$	$8.055x10^{-4}$
T≥65	$2.930x10^{-13}$	$-2.095x10^{-10}$	$6.006x10^{-8}$	$-9.147x10^{-6}$	$7.170x10^{-4}$

Table 2.6: MAE Values for Liquid Thermal Conductivity and Viscosity

Property	MAE (%)
k(T)	0.00466
μ(T)	0.03221

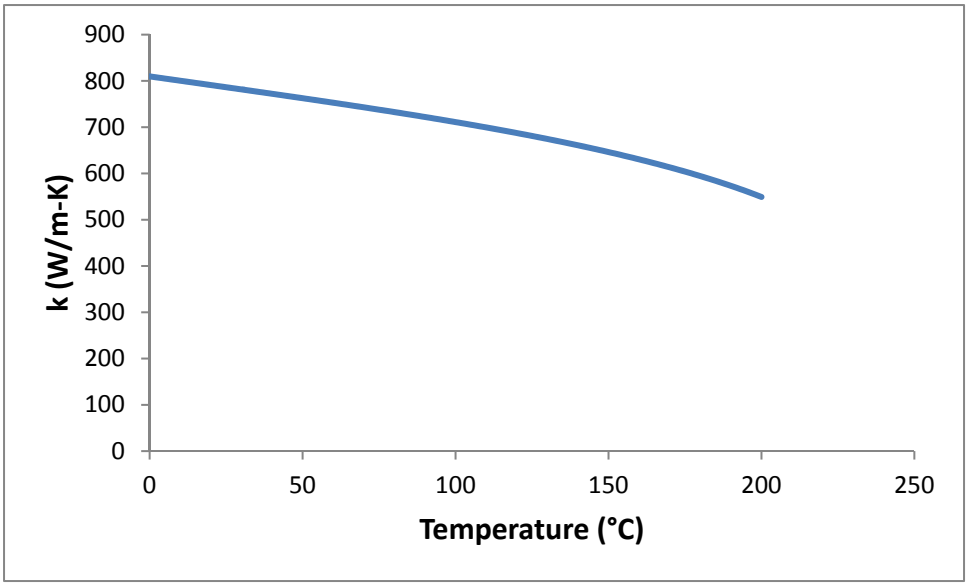

Figure 2.5: Methanol Liquid Thermal Conductivity

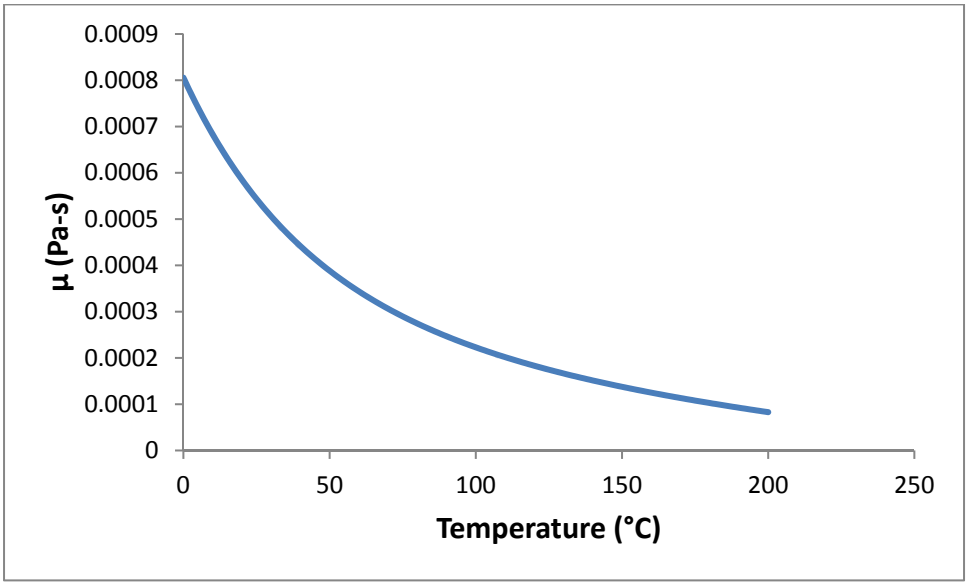

Figure 2.6: Methanol Liquid Viscosity

Methanol liquid enthalpy was assumed to be zero at its normal boiling point; this leads to a negative value of enthalpy for lower temperatures. The curve may be translated vertically by assuming a different zero enthalpy reference point if desired.

Table 2.7: Polynomial Coefficients for Liquid Enthalpy and Surface Tension

	$f(T)=a1*T^4+a2*T^3+a3*T^2+a4*T+a5$				
h(T)	a1	a2	a3	a4	a5
T<65	-4.890×10^{-6}	1.127×10^{-2}	2.264	2401.34	-1.672×10^{5}
T≥65	1.249×10^{-4}	-4.304×10^{-2}	10.813	1808.65	-1.521×10^{5}
σ(T)					
T<65	1.080×10^{-12}	-1.003×10^{-9}	7.229×10^{-8}	-8.456×10^{-5}	2.434×10^{-2}
T≥65	4.488×10^{-12}	-2.355×10^{-9}	2.789×10^{-7}	-9.863×10^{-5}	2.470×10^{-2}

Table 2.8: MAE Values for Liquid Enthalpy and Surface Tension

Property	MAE (%)
h(T)	0.05796
σ(T)	0.00665

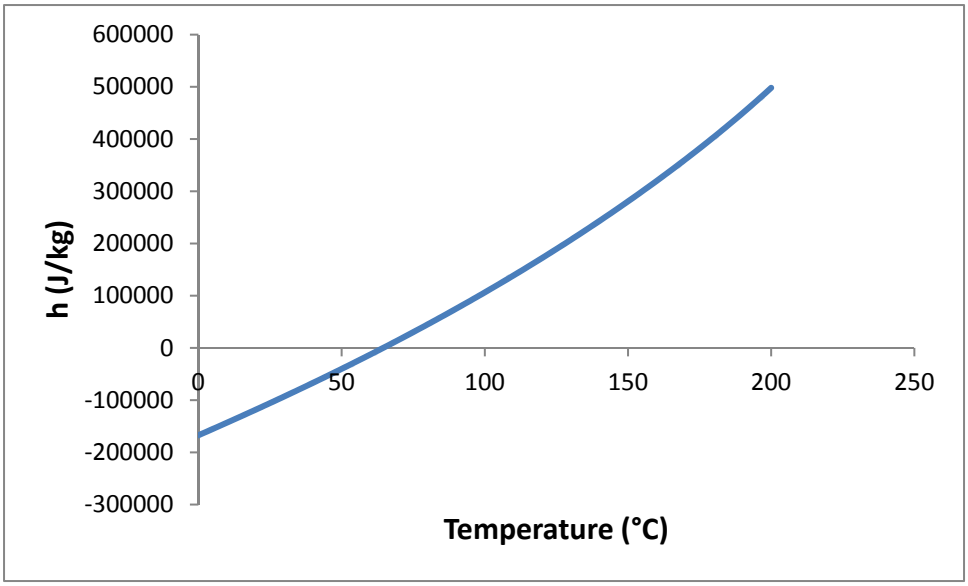

Figure 2.7: Methanol Liquid Enthalpy

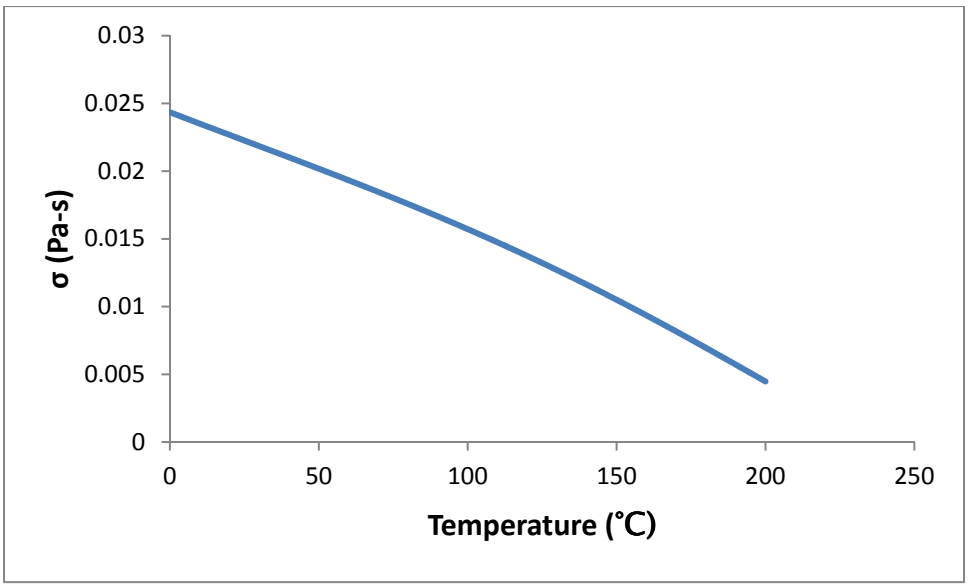

Figure 2.8: Methanol Liquid Surface Tension

Table 2.9: Summary of Polynomial Curve Fit Coefficients for Liquid Phase Methanol

	$f(T)=a1*T^4+a2*T^3+a3*T^2+a4*T+a5$				
ρ(T)	a1	a2	a3	a4	a5
T<65	-2.086×10^{-8}	-5.043×10^{-6}	2.214×10^{-4}	-0.9382	809.646
T≥65	-1.628×10^{-7}	5.755×10^{-5}	-9.929×10^{-3}	-0.2220	791.160
$c_p(T)$					
T<65	-1.474×10^{-7}	-2.639×10^{-6}	0.03263	4.532	2401.06
T≥65	9.634×10^{-6}	-4.203×10^{-3}	0.7156	-44.25	3678.00
k(T)					
T<65	1.051×10^{-11}	-7.967×10^{-9}	1.833×10^{-6}	-3.873×10^{-4}	0.2094
T≥65	2.505×10^{-11}	-1.468×10^{-8}	3.005×10^{-6}	-4.757×10^{-4}	0.2118
μ(T)					
T<65	4.667×10^{-12}	-1.218×10^{-9}	1.564×10^{-7}	-1.371×10^{-5}	8.055×10^{-4}
T≥65	2.930×10^{-13}	-2.095×10^{-10}	6.006×10^{-8}	-9.147×10^{-6}	7.170×10^{-4}
h(T)					
T<65	-4.890×10^{-6}	1.127×10^{-2}	2.264	2401.34	-1.672×10^{5}
T≥65	1.249×10^{-4}	-4.304×10^{-2}	10.813	1808.65	-1.521×10^{5}
σ(T)					
T<65	1.080×10^{-12}	-1.003×10^{-9}	7.229×10^{-8}	-8.456×10^{-5}	2.434×10^{-2}
T≥65	4.488×10^{-12}	-2.355×10^{-9}	2.789×10^{-7}	-9.863×10^{-5}	2.470×10^{-2}

Table 2.10: Summary of MAE of the Fluid Phase Methanol Polynomial Correlations

Property	MAE (%)
ρ(T)	0.00600
$c_p(T)$	0.08419
k(T)	0.00466
μ(T)	0.03221
h(T)	0.05796
σ(T)	0.00665

2.2.2 Vapor Phase

Vapor property routines for methanol were found by fitting 4th order polynomials to the REFPROP output. Coefficients for the vapor phase properties and MAE values are presented below.

Table 2.11: Polynomial Coefficients for Vapor Density and Specific Heat Capacity

	$f(T)=a1*T^4+a2*T^3+a3*T^2+a4*T+a5$				
$\rho_g(T)$	a1	a2	a3	a4	a5
T<65	$1.702x10^{-8}$	$9.066x10^{-7}$	$9.744x10^{-5}$	$3.413x10^{-3}$	$5.801x10^{-2}$
T≥65	$9.406x10^{-8}$	$-2.664x10^{-5}$	$3.872x10^{-3}$	$-2.280x10^{-1}$	5.361
$c_{pg}(T)$					
T<65	$1.013x10^{-5}$	$-1.222x10^{-3}$	$-2.904x10^{-2}$	26.683	2986.70
65≤T<166	$-2.368x10^{-5}$	$1.244x10^{-2}$	-2.100	164.454	-384.087
T≥166	$2.527x10^{-3}$	-1.791	474.143	$5.551x10^{4}$	$2.432x10^{6}$

Table 2.12: MAE Values for Vapor Density and Specific Heat Capacity

Property	MAE (%)
$\rho_g(T)$	0.09384
$c_{pg}(T)$	0.06776

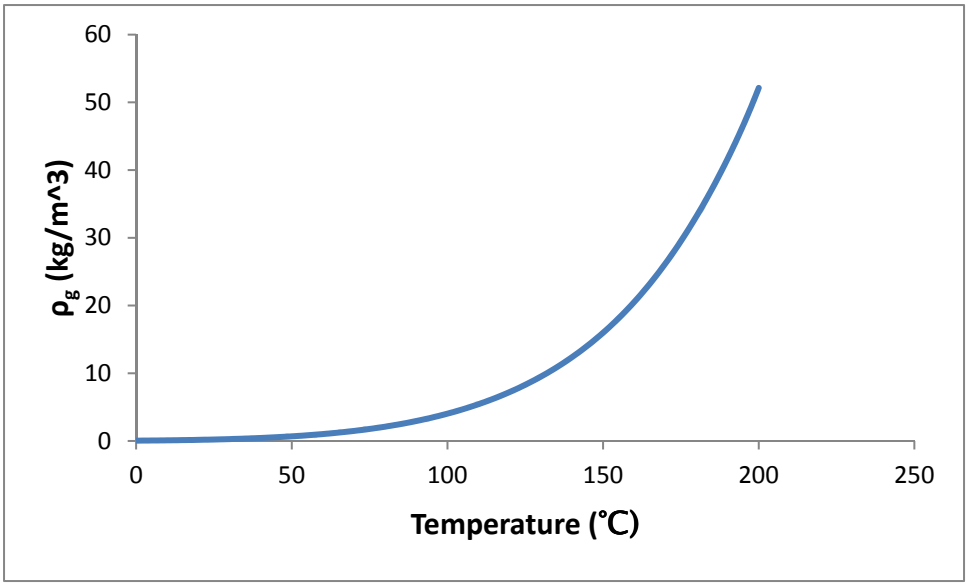

Figure 2.9: Methanol Vapor Density

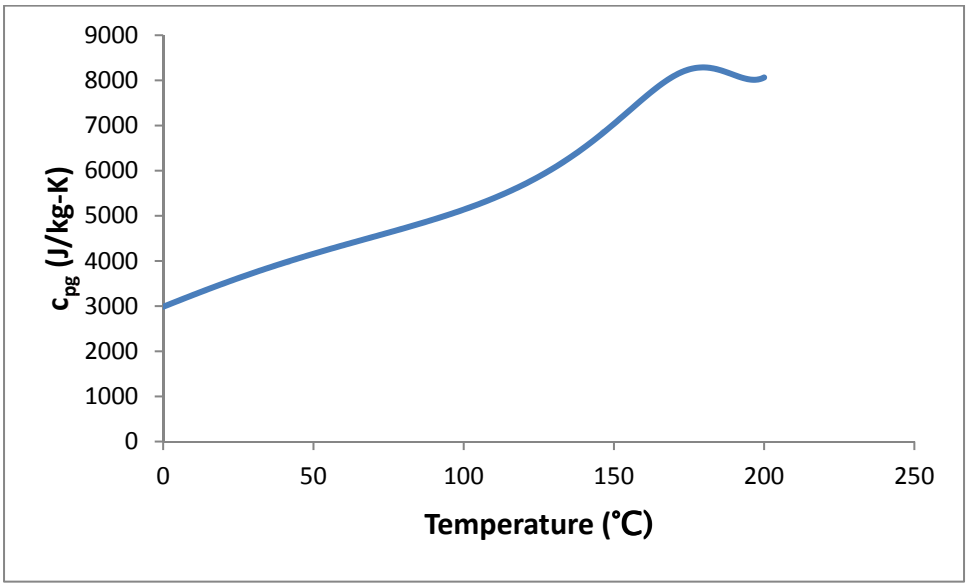

Figure 2.10: Methanol Vapor Specific Heat Capacity

Table 2.13: Polynomial Coefficients for Vapor Thermal Conductivity and Viscosity

	$f(T)=a1*T^4+a2*T^3+a3*T^2+a4*T+a5$				
$k_g(T)$	a1	a2	a3	a4	a5
$T<65$	$1.086x10^{-11}$	$8.705x10^{-10}$	$2.055x10^{-7}$	$8.843x10^{-5}$	$1.309x10^{-2}$
$T\geq65$	$-1.022x10^{-10}$	$6.297x10^{-8}$	$-1.137x10^{-5}$	$9.853x10^{-4}$	$-1.160x10^{-3}$
$\mu_g(T)$					
$T<65$	$-1.215x10^{-16}$	$-1.382x10^{-13}$	$-1.626x10^{-12}$	$3.139x10^{-8}$	$8.839x10^{-6}$
$T\geq65$	$1.495x10^{-14}$	$-6.613x10^{-12}$	$1.040x10^{-9}$	$-4.200x10^{-8}$	$1.073x10^{-5}$

Table 2.14: MAE Values for Vapor Thermal Conductivity and Viscosity

Property	MAE (%)
$k_g(T)$	0.20173
$\mu_g(T)$	0.02945

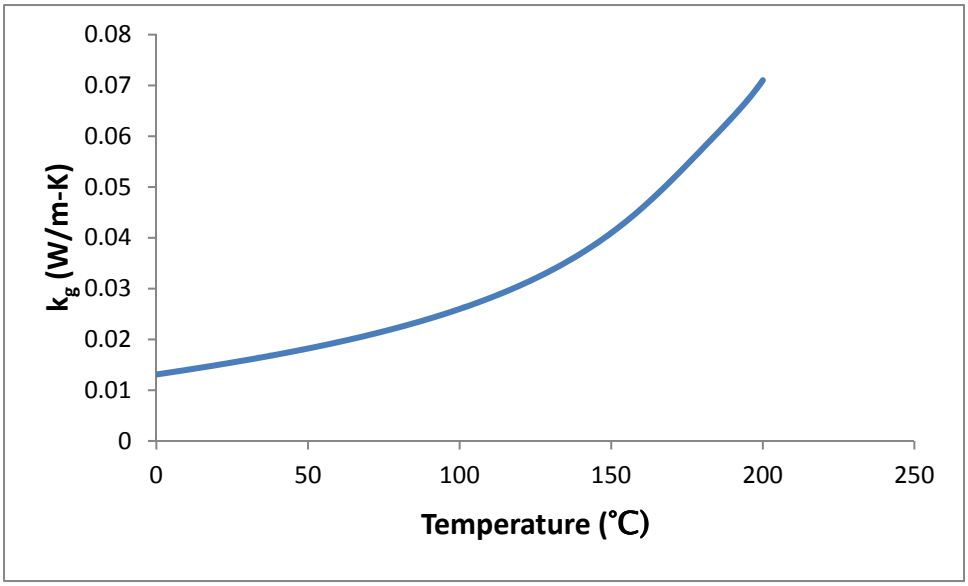

Figure 2.11: Methanol Vapor Thermal Conductivity

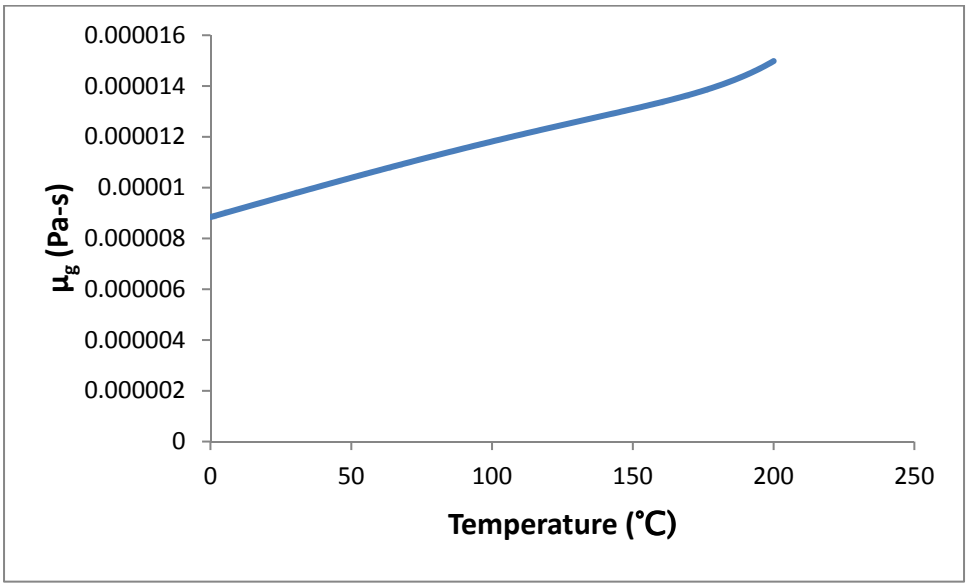

Figure 2.12: Methanol Vapor Viscosity

Table 2.15: Polynomial Coefficients for Vapor Enthalpy and Saturation Pressure

	$f(T)=a1*T^4+a2*T^3+a3*T^2+a4*T+a5$				
$h_g(T)$	a1	a2	a3	a4	a5
$T<65$	$-1.011x10^{-4}$	$6.035x10^{-3}$	$-9.726x10^{-1}$	1045.05	$1.038x10^{6}$
$65\leq T<155$	$-3.673x10^{-5}$	$-2.225x10^{-2}$	3.355	762.307	$1.044x10^{6}$
$T\geq 155$	$-7.448x10^{-2}$	5.361	-1441.16	$1.714x10^{5}$	$-6.446x10^{6}$
Psat(T)					
$T<65$	$1.724x10^{-3}$	$6.924x10^{-2}$	7.876	250.19	4056.23
$T\geq 65$	$2.129x10^{-3}$	$7.893x10^{-2}$	-9.315	2079.1	$5.288x10^{4}$

Table 2.16: MAE Values for Vapor Enthalpy and Saturation Pressure

Property	MAE (%)
$h_g(T)$	0.00165
Psat(T)	0.05705

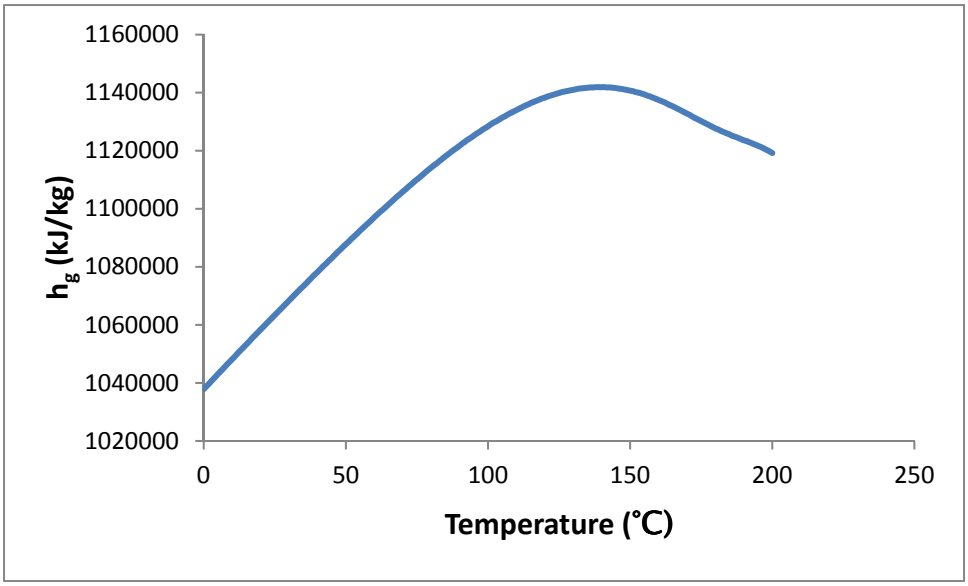

Figure 2.13: Methanol Vapor Enthalpy

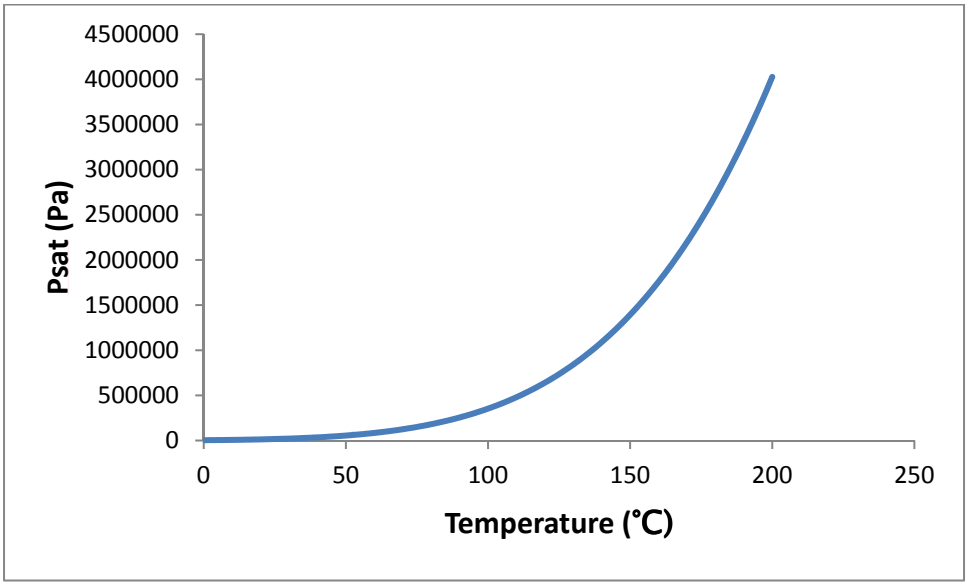

Figure 2.14: Methanol Saturation Pressure

Table 2.17: Summary of Polynomial Curve Fit Coefficients for Vapor Phase Methanol

	$f(T)=a1*T^4+a2*T^3+a3*T^2+a4*T+a5$				
$\rho_g(T)$	a1	a2	a3	a4	a5
T<65	$1.702x10^{-8}$	$9.066x10^{-7}$	$9.744x10^{-5}$	$3.413x10^{-3}$	$5.801x10^{-2}$
T≥65	$9.406x10^{-8}$	$-2.664x10^{-5}$	$3.872x10^{-3}$	$-2.280x10^{-1}$	5.361
$c_{pg}(T)$					
T<65	$1.013x10^{-5}$	$-1.222x10^{-3}$	$-2.904x10^{-2}$	26.683	2986.70
65≤T<166	$-2.368x10^{-5}$	$1.244x10^{-2}$	-2.100	164.454	-384.087
T≥166	$2.527x10^{-3}$	-1.791	474.143	$5.551x10^{4}$	$2.432x10^{6}$
$k_g(T)$					
T<65	$1.086x10^{-11}$	$8.705x10^{-10}$	$2.055x10^{-7}$	$8.843x10^{-5}$	$1.309x10^{-2}$
T≥65	$-1.022x10^{-10}$	$6.297x10^{-8}$	$-1.137x10^{-5}$	$9.853x10^{-4}$	$-1.160x10^{-3}$
$\mu_g(T)$					
T<65	$-1.215x10^{-16}$	$-1.382x10^{-13}$	$-1.626x10^{-12}$	$3.139x10^{-8}$	$8.839x10^{-6}$
T≥65	$1.495x10^{-14}$	$-6.613x10^{-12}$	$1.040x10^{-9}$	$-4.200x10^{-8}$	$1.073x10^{-5}$
$h_g(T)$					
T<65	$-1.011x10^{-4}$	$6.035x10^{-3}$	$-9.726x10^{-1}$	1045.05	$1.038x10^{6}$
65≤T<155	$-3.673x10^{-5}$	$-2.225x10^{-2}$	3.355	762.307	$1.044x10^{6}$
T≥155	$-7.448x10^{-2}$	5.361	-1441.16	$1.714x10^{5}$	$-6.446x10^{6}$
Psat(T)					
T<65	$1.724x10^{-3}$	$6.924x10^{-2}$	7.876	250.19	4056.23
T≥65	$2.129x10^{-3}$	$7.893x10^{-2}$	-9.315	2079.1	$5.288x10^{4}$

Table 2.18: Summary of MAE of the Vapor Phase Methanol Polynomial Correlations

Property	MAE (%)
$\rho_g(T)$	0.09384
$c_{pg}(T)$	0.06776
$k_g(T)$	0.20173
$\mu_g(T)$	0.02945
$h_g(T)$	0.00165
Psat(T)	0.05705

2.3 Methanol-Water Mixtures

Again, the NIST REFPROP 9.0 database served as the basis for determining mixture properties for the binary water/methanol mixture. The mixing rules used rely on one of these three composition bases: mass fraction, w, molar fraction, x, and volume fraction, Φ.

$$w_i = \frac{m_i}{m_{tot}} \tag{2.1}$$

$$x_i = \frac{n_i}{n_{tot}} \tag{2.2}$$

$$\Phi_i = \frac{V_i}{V_{tot}} \tag{2.3}$$

For this study, all properties are determined using subroutines explicit in molar fraction. If a mixing rule requires a different basis, molar fraction must be converted. Converting from molar fraction to mass fraction, molar fraction is multiplied by the ratio of individual molecular weight to mixture molecular weight.

$$w_i = x_i \cdot \frac{M_i}{M_{tot}} \tag{2.4}$$

The following equation shows the conversion from molar fraction to volume fraction.

$$\Phi_i = \frac{x_i V_{mi}}{\sum_{i=1}^{2} x_i V_{mi}} \tag{2.5}$$

In the above equation, V_m is defined as the molar volume.

$$V_m = \frac{M}{\rho} \tag{2.6}$$

Most mixture properties can be determined using a linear mixing rule with either a molar-based composition, x, or a mass-based composition, w. Figure 2.15 illustrates the difference caused by using one composition over the other; one curve is linear while the other is nonlinear. Whether to use a mass or molar basis must be tested for each individual case; there is no apparent trend regarding whether the mass or molar based correlation leads to a linear correlation. For properties not adequately described using a linear average, mixing rules recommended by Perry's Chemical Engineers' Handbook [20] and other sources were employed. Some property values were neither calculated by the REFPROP program nor derived empirically. If experimental data could be found, the correlation was validated against available information; otherwise the uncertainty listed is the expected uncertainty listed by the source in which the mixing rule was found.

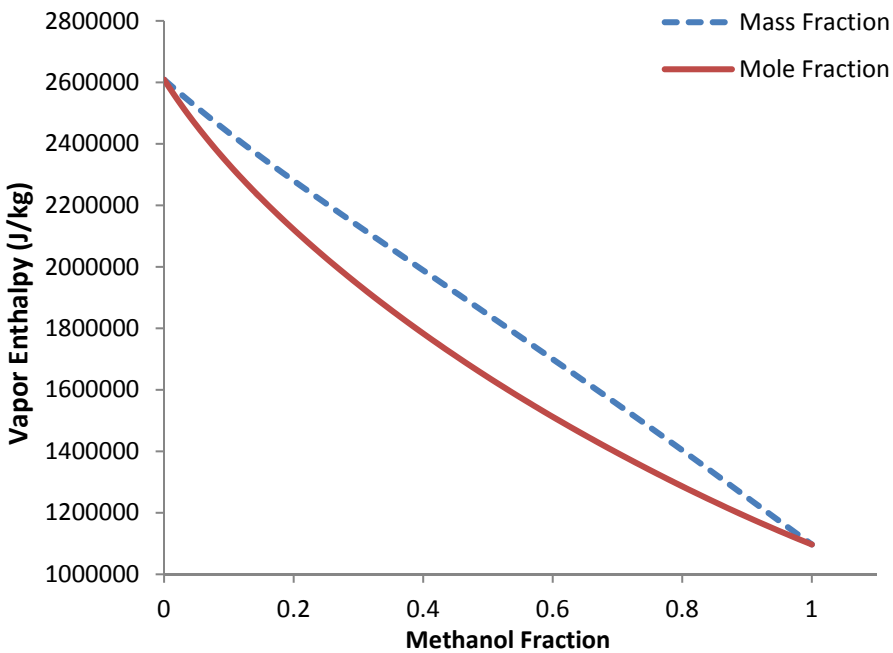

Figure 2.15: Comparing Effects of Mass and Molar Basis on the Linearity of Vapor Enthalpy

2.3.1 Liquid Phase

Table 2.19: Summary of Liquid Phase Mixing Rules

Property	Source	Correlation	Uncertainty
$\rho_f(T,x)$	[20]	$\frac{1}{\rho_m} = \sum_{i=1}^{2} \frac{x_i}{\rho_i}$	0.46%
$\sigma(T,x)$		$\sigma_m = \sum_{i=1}^{2} w_i \sigma_i$	2.7%
$c_{pf}(T,x)$	[20]	$c_{pm} = \sum_{i=1}^{2} w_i c_{pi}$	0.45%
$h_f(T,x)$		$h_m = \sum_{i=1}^{2} x_i h_i$	0.16%
$\mu_f(T,x)$	[21][22]	$\mu_m = \Phi_{org}\mu_{org} \exp(\Phi_{H_2O}\alpha_{H_2O}) + \Phi_{H_2O}\mu_{H_2O} \exp(\Phi_{org}\alpha_{org})$	8%
$k_f(T,x)$	[20]	$k_m = \sum_{i=1}^{2}\sum_{j=1}^{2} \Phi_i \Phi_j \frac{2k_i k_j}{k_i + k_j}$	4-8%

Liquid mixture density employs the Li correlation as found in the above table [20]. Both the correlation and a simple linear mixing rule were tested with both mass and molar fraction as the basis. It was found that the Li correlation using a molar fraction basis achieved the best agreement with the REFPROP output with an MAE value of 0.46%

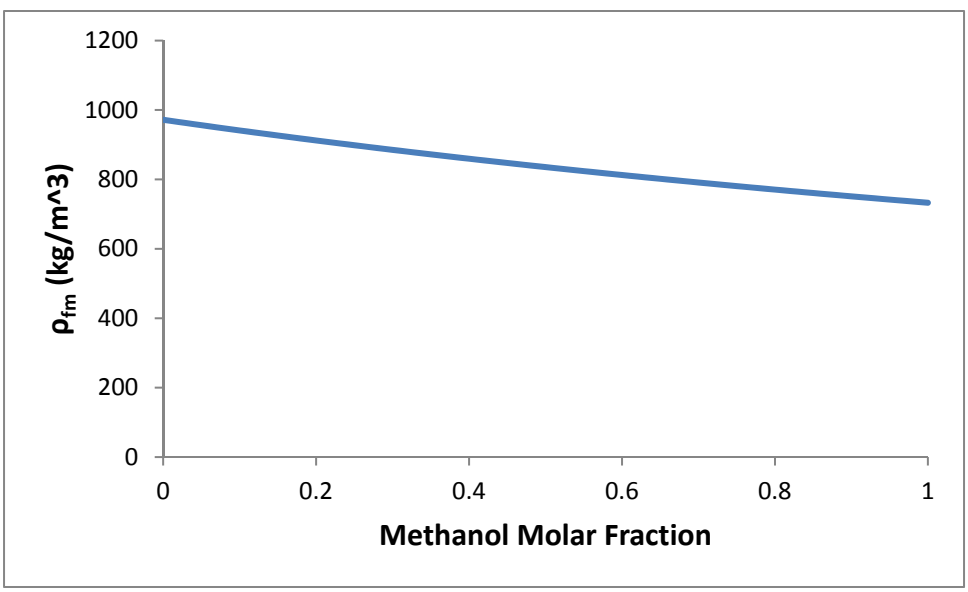

Figure 2.16: Liquid Mixture Density

Liquid mixture surface tension, specific heat capacity, and enthalpy are all able to be described by a linear mixing rule. Here, surface tension and specific heat capacity have MAE values of 2.7% and 0.45% respectively.

$$\sigma_m = \sum_{i=1}^{2} w_i \sigma_i \tag{2.7}$$

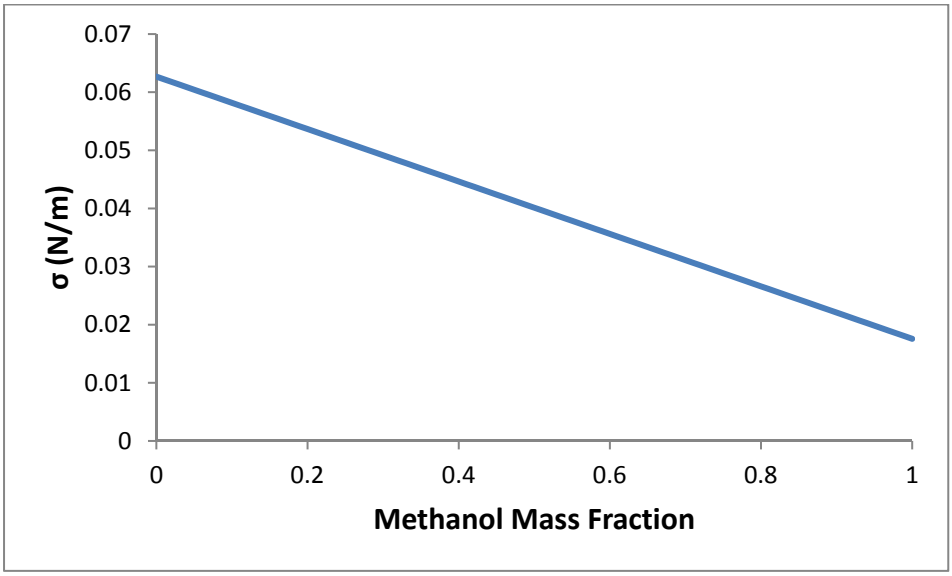

Figure 2.17: Liquid Mixture Surface Tension

$$c_{pm} = \sum_{i=1}^{2} w_i c_{pi} \tag{2.8}$$

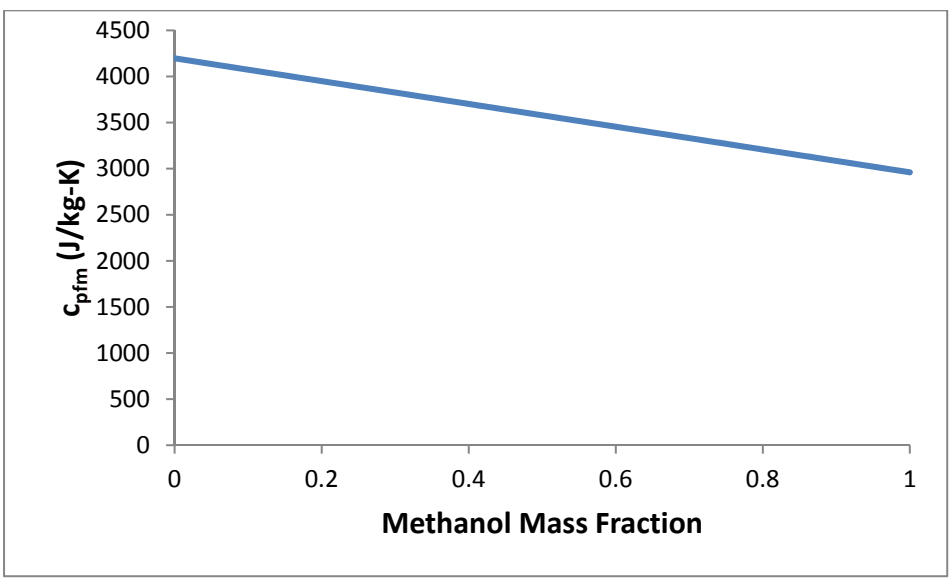

Figure 2.18: Liquid Mixture Specific Heat Capacity

For liquid mixture enthalpy, a linear mixing rule with a molar basis achieved the best agreement with the NIST data; an MAE value of 0.16% was achieved. This may be counter intuitive since enthalpy is J/kg, a mass based property.

$$h_m = \sum_{i=1}^{2} x_i h_i \tag{2.9}$$

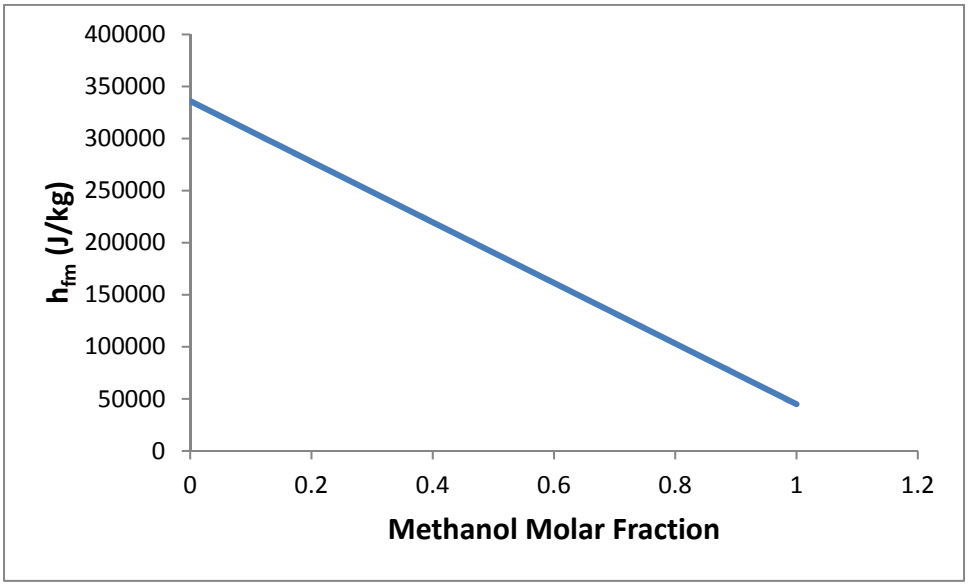

Figure 2.19: Liquid Mixture Enthalpy

The NIST database is unable to calculate the following transport properties that are needed for the numerical simulation: viscosity, μ, and thermal conductivity k. Correlations to evaluate mixture viscosity in the liquid phase were developed based on mixing rules reported in literature from the fields of analytical chemistry and high performance liquid chromatography. Studies conducted by Li and Carr [21] and Billen, et al [22] have found a good agreement between experimental data obtained by Colin, et al [23] and predictions of the Lobe correlation illustrated in Equation (2.10) and seen in Figure 2.20.

$$\mu_m = \Phi_{org}\mu_{org}\exp\left(\Phi_{H_2O}\alpha_{H_2O}\right) + \Phi_{H_2O}\mu_{H_2O}\exp\left(\Phi_{org}\alpha_{org}\right) \tag{2.10}$$

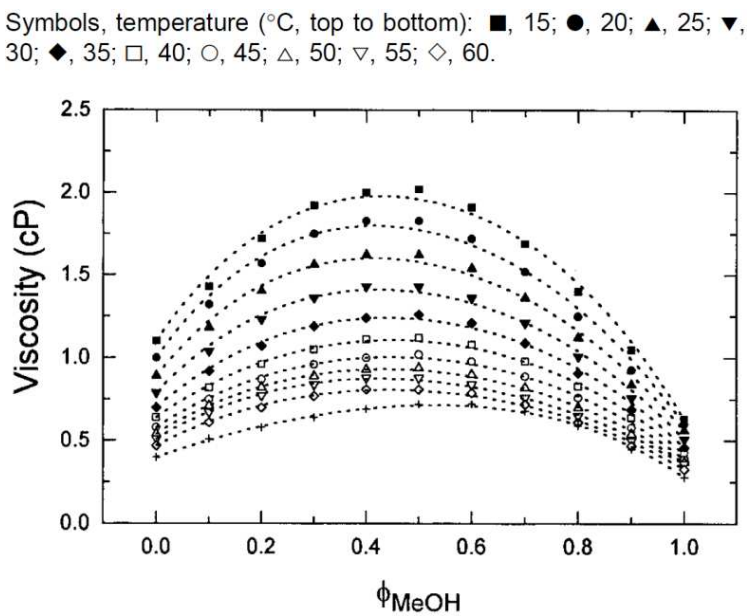

Figure 2.20: Lobe Correlation Curves Fitted to Experimental Data [21]

While the Lobe correlation does an excellent job of fitting experimental data, the values for the coefficients, α, cannot be predicted; it is important to obtain experimental results for the range of temperatures being investigated. The current subroutine is applicable only for temperatures which have experimental data available. The next figure shows a graph of the tabulated lobe coefficients in the study by Li and Carr [21] as a function of temperature.

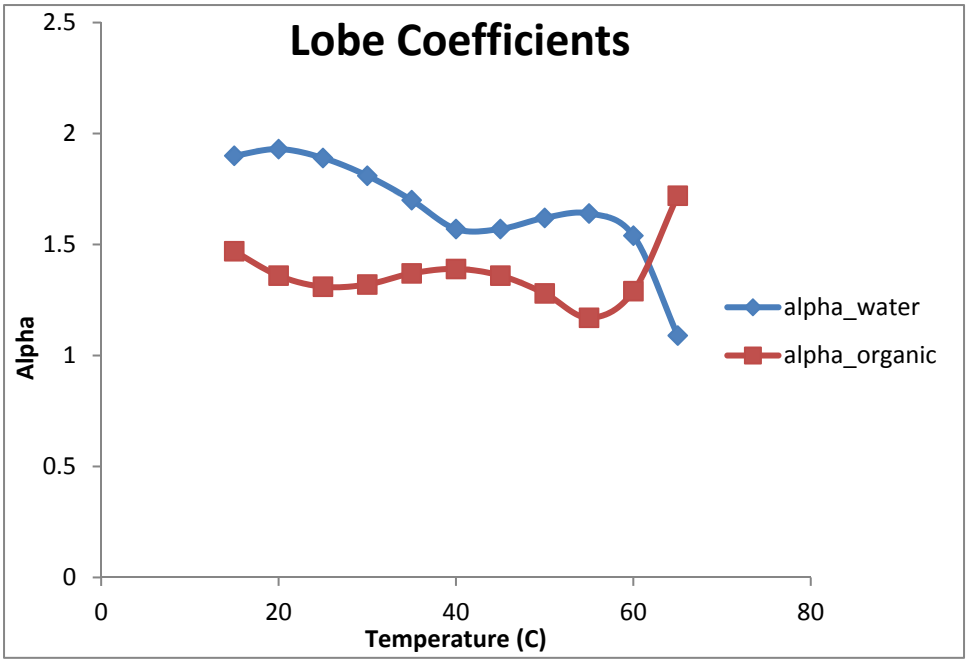

Figure 2.21: Graph of Lobe Coefficients for Water and Methanol

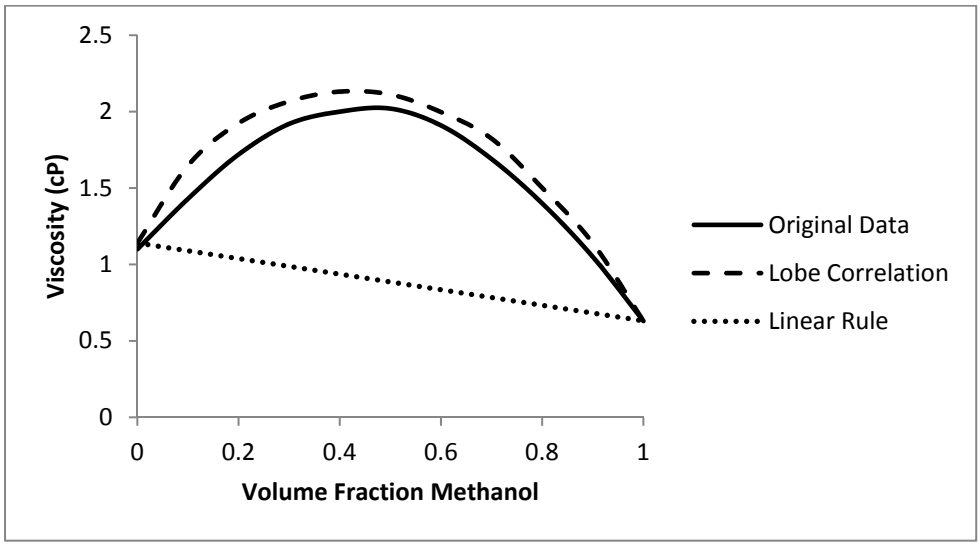

Figure 2.22: Comparison of Mixing Rules for Liquid Mixture Viscosity

The previous figure shows the difference between using a linear mixing rule and the Lobe correlation. The solid line represents the original experimental data points while the dashed line is the output of the liquid viscosity correlation. The fine dotted line is the result of using a linear mixing rule. For this case, the MAE for the Lobe correlation was 7% while the linear rule yielded an MAE value of 38%. Errors reached as high as 56% for the linear rule as seen in the following table.

Table 2.20: Comparison Viscosity Values for Lobe Correlation and Linear Mixing Rules

φ	μ (cP)	Lobe	% Error	Linear	% Error
0	1.1	1.140	3.675	1.140	3.675
0.1	1.43	1.648	15.21	1.090	23.81
0.2	1.72	1.924	11.89	1.039	39.62
0.3	1.92	2.067	7.646	0.9877	48.56
0.4	2	2.131	6.542	0.9367	53.16
0.5	2.02	2.112	4.551	0.8858	56.15
0.6	1.91	1.997	4.557	0.8349	56.29
0.7	1.69	1.823	7.895	0.7840	53.61
0.8	1.4	1.501	7.247	0.7330	47.64
0.9	1.05	1.140	8.544	0.6821	35.03
1	0.63	0.6312	0.190567	0.6312	0.1906
			Lobe		Linear
		MAE (%)	7.086		37.98

Liquid thermal conductivity is determined using a mixing rule found in Perry's Chemical Engineers' Handbook [20]. This mixing rule, the Spencer-Danner-Li correlation [24] [25], is a function of pure component thermal conductivity and volume fraction. Although, experimental data was not available for methanol-water mixtures, the expected uncertainty is listed as being 4-8%

$$k_m = \sum_{i=1}^{2}\sum_{j=1}^{2} \Phi_i \Phi_j \frac{2k_i k_j}{k_i + k_j} \tag{2.11}$$

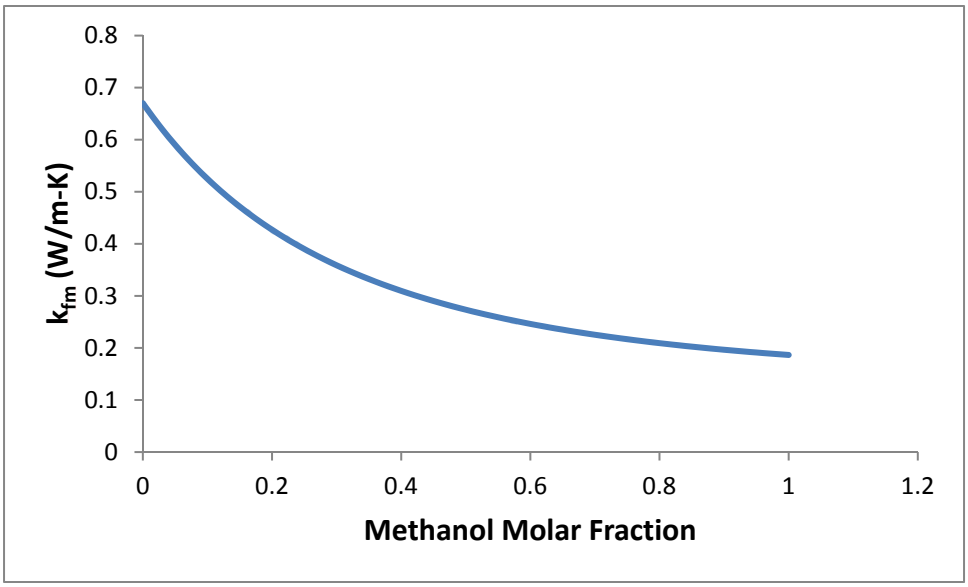

Figure 2.23: Liquid Mixture Thermal Conductivity

2.3.2 Vapor Phase

Table 2.21: Summary of Vapor Phase Mixing Rules

Property	Source	Correlation	Uncertainty
ρ_g(T,x)	[20]	$\frac{1}{\rho_m} = \sum_{i=1}^{2} \frac{w_i}{\rho_i}$	0.47%
c_{pg}(T,x)	[20]	$c_{pm} = \sum_{i=1}^{2} x_i c_{pi}$	4%
h_g(T,x)		$h_m = \sum_{i=1}^{2} w_i h_i$	0.51%
μ_g(T,x)	[26]	$\mu_m = \frac{\mu_g^c}{1+\varphi_{c,aw}\left[\frac{x_g^{aw}}{x_g^c}\right]} + \frac{\mu_g^{aw}}{1+\varphi_{aw,c}\left[\frac{x_g^c}{x_g^{aw}}\right]}$ $\varphi_{c,aw} = \frac{\left[1+\left(\mu_g^c/\mu_g^{aw}\right)^{\frac{1}{2}}(M_{wt}^{aw}/M_{wt}^c)^{\frac{1}{4}}\right]^2}{[8(1+M_{wt}^c/M_{wt}^{aw})]^{\frac{1}{2}}}$ $\varphi_{aw,c} = \frac{\left[1+\left(\mu_g^{aw}/\mu_g^c\right)^{\frac{1}{2}}(M_{wt}^{aw}/M_{wt}^c)^{\frac{1}{4}}\right]^2}{[8(1+M_{wt}^{aw}/M_{wt}^c)]^{\frac{1}{2}}}$	2-4%
k_g(T,x)	[27]	$k_m = \sum_{i=1}^{n} \frac{x_i k_i}{\sum_{j=1}^{n} x_j \varphi_{ij}}$	5-8%

Vapor mixture density employs the Li correlation as found in the previous table [20]. Both the correlation and a simple linear mixing rule were tested with both mass and molar fraction as the basis. It was found that the Li correlation using a mass fraction basis achieved the best agreement with the REFPROP output with an MAE value of 0.47%.

$$\frac{1}{\rho_m} = \sum_{i=1}^{2} \frac{w_i}{\rho_i} \tag{2.12}$$

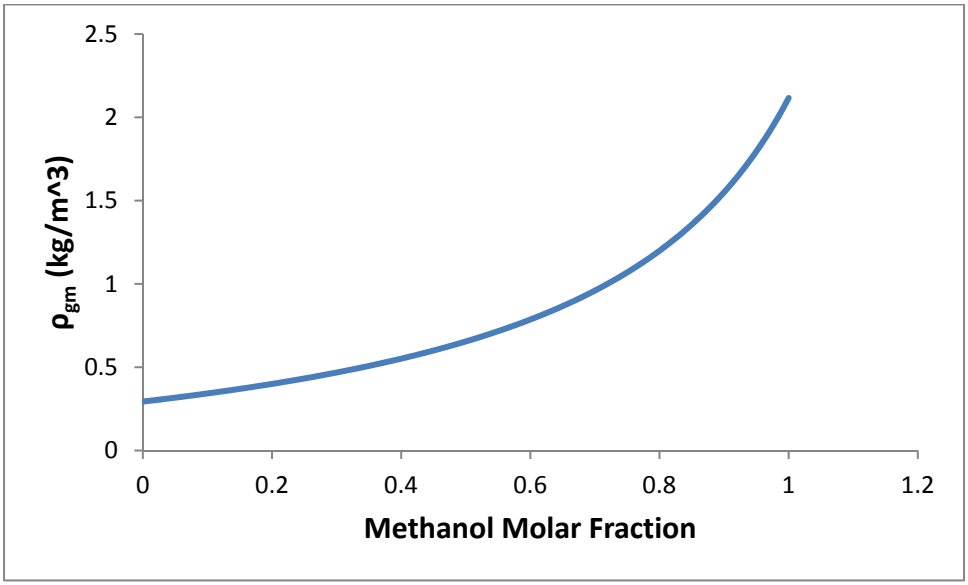

Figure 2.24: Vapor Mixture Density

Linear mixing rules were used for both mixture vapor specific heat capacity and enthalpy. An expected uncertainty of 4% is expected for c_p and an MAE value of 0.51% for enthalpy.

$$c_{pm} = \sum_{i=1}^{2} x_i c_{pi} \tag{2.13}$$

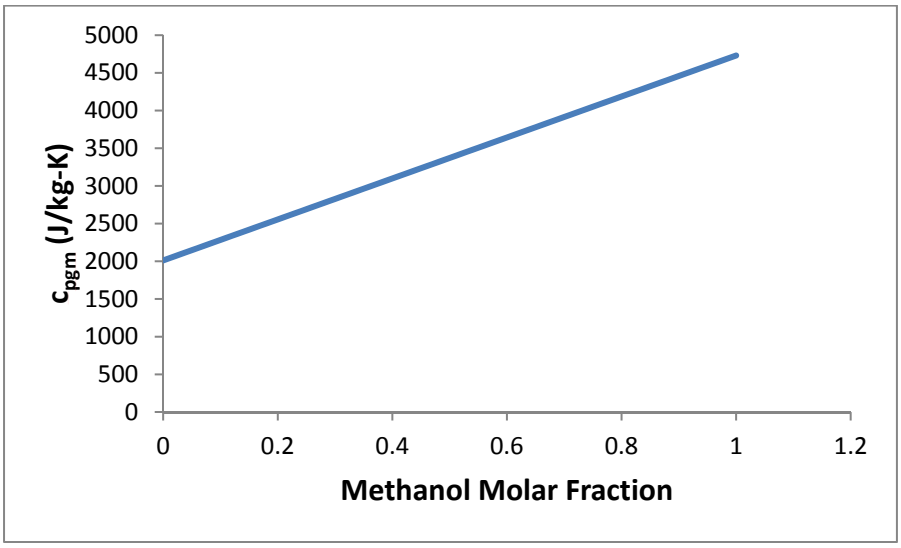

Figure 2.25: Vapor Mixture Specific Heat Capacity

$$h_m = \sum_{i=1}^{2} w_i h_i \tag{2.14}$$

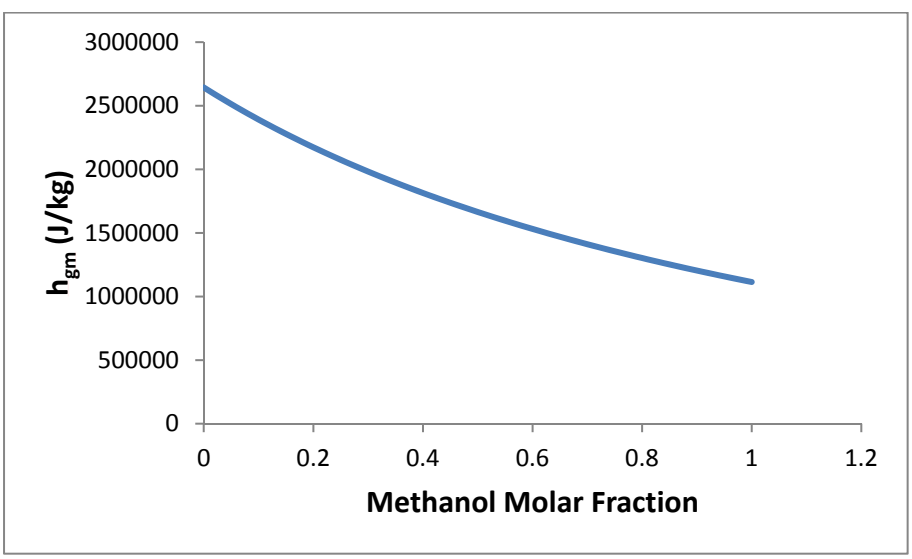

Figure 2.26: Vapor Mixture Enthalpy

For vapor phase mixture viscosity, documentation for the T2VOC program developed by UC Berkeley was used [26]. T2VOC is a numerical simulator for three-phase, three-component mixtures of air, water, and a volatile organic compound. Here, a modified version of the Wilke method [28] is employed to calculate vapor mixture viscosity. A mole fraction composition based mixing rule (2.15) is modified by the inclusion of two interaction parameters (2.16) and (2.17) these variables attempt to account for the effects of molecule size on the value of mixture viscosity. It is important to differentiate between Φ which stands for volume fraction of the mixture and φ which is the symbol used for interaction parameters in this study.

$$\mu_m = \frac{\mu_g^c}{1 + \varphi_{c,aw}\left[\frac{x_g^{aw}}{x_g^c}\right]} + \frac{\mu_g^{aw}}{1 + \varphi_{aw,c}\left[\frac{x_g^c}{x_g^{aw}}\right]} \tag{2.15}$$

$$\varphi_{c,aw} = \frac{\left[1 + \left(\mu_g^c/\mu_g^{aw}\right)^{\frac{1}{2}}(M_{wt}^{aw}/M_{wt}^c)^{\frac{1}{4}}\right]^2}{[8(1 + M_{wt}^c/M_{wt}^{aw})]^{\frac{1}{2}}} \tag{2.16}$$

$$\varphi_{aw,c} = \frac{\left[1 + \left(\mu_g^{aw}/\mu_g^c\right)^{\frac{1}{2}}(M_{wt}^{aw}/M_{wt}^c)^{\frac{1}{4}}\right]^2}{[8(1 + M_{wt}^{aw}/M_{wt}^c)]^{\frac{1}{2}}} \tag{2.17}$$

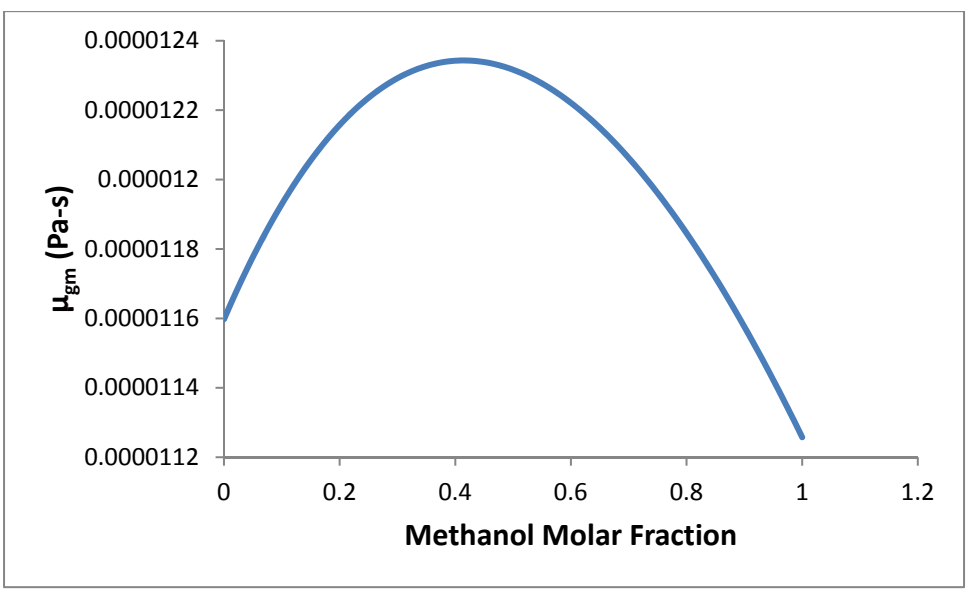

Figure 2.27: Methanol Vapor Mixture Viscosity

Vapor thermal conductivity is determined using a mixing rule from the Properties of Gases and Liquids [27]. This correlation uses the Wassiljewa equation (2.18) with the modification suggested by Mason and Saxena[29]. The interaction parameter in this case is similar to the one used for vapor mixture viscosity when $i \neq j$. When the values for i and j are equal, the value of the interaction parameter is 1.

$$k_m = \sum_{i=1}^{n} \frac{x_i k_i}{\sum_{j=1}^{n} x_j \varphi_{ij}} \tag{2.18}$$

The above correlation is mostly suited for use with non-polar mixtures; the expected uncertainty is usually less than 3-4%. However, for mixtures involving polar molecules, such as water or alcohols, this error rises to over 5-8%.

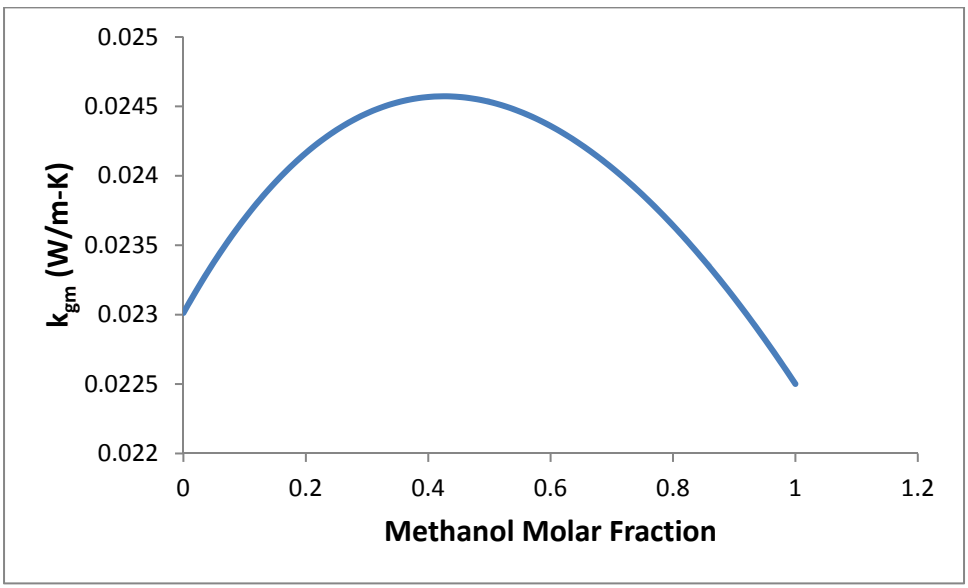

Figure 2.28: Methanol Vapor Mixture Thermal Conductivity

2.3.3 Phase Diagram Properties

For a pure substance, the temperature of the vapor and liquid phases is the same at saturation and this temperature remains constant throughout the boiling process. However, both the temperature and composition of a mixture changes as fluid evaporates. A typical phase diagram for a binary mixture is presented in Figure 2.29.

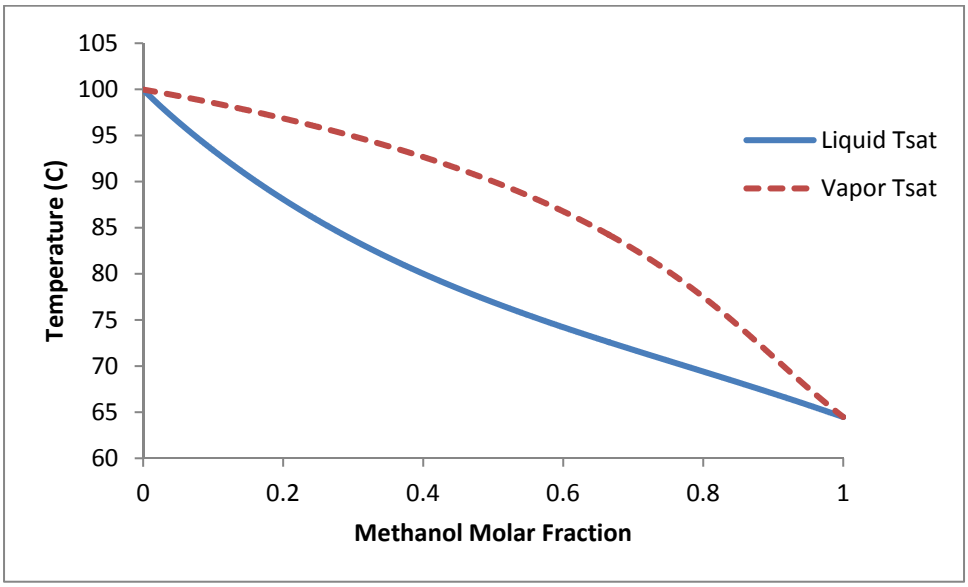

Figure 2.29: Phase Diagram for Binary Methanol/Water Mixture at 1 atm.

A program for recreating the methanol-water phase diagram was developed using the REFPROP program. A polynomial curve was fitted to the phase diagram for a range of pressures from 1-3 bar. For this correlation, Tsat is a 6th order polynomial function of mixture composition and the coefficients are themselves 4th order polynomial functions of pressure. The inverse of the saturation temperature correlations were also developed by using the bisection method to solve for both liquid and vapor mixture composition as a function of mixture temperature and pressure.

Table 2.22: Polynomial Curve Fit Coefficients for Liquid Phase Saturation Temperature

		$f(x)=a1*x^6+a2*x^5+a3*x^4+a4*x^3+a5*x^2+a6*x+a7$					
$Tsat_f(x,P)$	a1	a2	a3	a4	a5	a6	a7
P = 1 bar	106.2	-398.9	629.9	-559.5	314.6	-128.1	99.61
		$f(P)=b1*P^4+b2*P^3+b3*P^2+b4*P+b5$					
		b1	b2	b3	b4	b5	
P < 3 bar	a1	1.466	-15.15	62.84	-139.6	197.0	
	a2	-5.128	53.02	-220.5	493.5	-719.8	
	a3	7.131	-73.87	308.3	-697.5	1085.9	
	a4	-4.997	51.90	-217.7	501.0	-889.7	
	a5	1.793	-18.69	79.01	-186.4	438.8	
	a6	-0.2255	2.354	-9.975	23.73	-144.0	
	a7	-0.4565	4.851	-21.33	57.49	59.06	

Table 2.23: Polynomial Curve Fit Coefficients for Vapor Phase Saturation Temperature

		$f(x)=a1*x^6+a2*x^5+a3*x^4+a4*x^3+a5*x^2+a6*x+a7$					
$Tsat_g(x,P)$	a1	a2	a3	a4	a5	a6	a7
P = 1 bar	10.32	24.21	-67.92	39.87	-18.38	-23.50	99.61
		$f(P)=b1*P^4+b2*P^3+b3*P^2+b4*P+b5$					
		b1	b2	b3	b4	b5	
P < 3 bar	a1	1.106	-11.17	44.43	-88.38	64.33	
	a2	-2.879	28.92	-113.84	219.97	-107.96	
	a3	2.691	-26.84	104.29	-194.13	46.07	
	a4	-1.149	11.40	-43.82	79.29	-5.852	
	a5	0.2372	-2.355	9.082	-16.74	-8.608	
	a6	0.03507	-0.3835	1.768	-5.290	-19.63	
	a7	-0.4565	4.851	-21.33	57.49	59.06	

Table 2.24: MAE Values for Saturation Temperature Routines

Property	MAE (%)
$Tsat_f(x,P)$	0.018241
$Tsat_g(x,P)$	0.014008

2.3.4 Quality

As heat is applied to a liquid it will begin to evaporate and if sufficient heat is supplied, the liquid begins to boil; the liquid becomes a two-phase mixture of both vapor and liquid. Quality is defined as the mass fraction of vapor in a saturated two-phase mixture. A subroutine was developed using the REFPROP program which calculates quality as a function of total mixture enthalpy, initial liquid composition, and pressure. The quality program agrees very well with the REFPROP output having an MAE value of 0.46882%.

Table 2.25: Polynomial Curve Fit Coefficients for Mixture Quality

Qual(h,x,P)	$f(h)=a1*h^2+a2*h+a3$
a1	$f(x)=b1*x^4+b2*x^3+b3*x^2+b4*x+b5$
a2	$f(x)=c1*x^4+c2*x^3+c3*x^2+c4*x+c5$
a3	$f(x)=d1*x^4+d2*x^3+d3*x^2+d4*x+d5$

	$f(P)=e1*P+e2*P+e3*P+e4*P+e5$				
	e1	e2	e3	e4	e5
b1	0.0	$-1.335*10^{-14}$	$6.941*10^{-14}$	$-1.967*10^{-15}$	$-9.689*10^{-13}$
b2	0.0	$3.383*10^{-14}$	$-1.862*10^{-13}$	$1.192*10^{-13}$	$2.105*10^{-12}$
b3	0.0	$-2.892*10^{-14}$	$1.700*10^{-13}$	$-2.069*10^{-13}$	$-1.016*10^{-12}$
b4	0.0	$9.292*10^{-15}$	$-5.888*10^{-14}$	$1.023*10^{-13}$	$-1.172*10^{-13}$
b5	$6.468*10^{-16}$	$-5.930*10^{-15}$	$1.972*10^{-14}$	$-2.728*10^{-14}$	$2.528*10^{-15}$
c1	0.0	$3.313*10^{-08}$	$-1.942*10^{-07}$	$2.190*10^{-07}$	$1.690*10^{-06}$
c2	0.0	$-7.999*10^{-08}$	$4.780*10^{-07}$	$-6.404*10^{-07}$	$-3.046*10^{-06}$
c3	0.0	$6.270*10^{-08}$	$-3.799*10^{-07}$	$5.651*10^{-07}$	$9.178*10^{-07}$
c4	0.0	$-1.693*10^{-08}$	$1.019*10^{-07}$	$-1.351*10^{-07}$	$8.830*10^{-07}$
c5	0.0	$2.125*10^{-09}$	$-1.531*10^{-08}$	$4.336*10^{-08}$	$4.298*10^{-07}$
d1	0.0	$-1.111*10^{-02}$	$6.971*10^{-02}$	$-1.096*10^{-01}$	$-4.649*10^{-01}$
d2	0.0	$2.278*10^{-02}$	$-1.345*10^{-01}$	$1.572*10^{-01}$	$9.030*10^{-01}$
d3	0.0	$-1.250*10^{-02}$	$5.862*10^{-02}$	$5.112*10^{-02}$	$-4.537*10^{-01}$
d4	0.0	0.0	$1.069*10^{-02}$	$-1.113*10^{-01}$	$2.068*10^{-01}$
d5	0.0	0.0	$7.563*10^{-03}$	$-6.812*10^{-02}$	$-1.270*10^{-01}$

Table 2.26: MAE Values of Quality Subroutine

Property	MAE (%)
Qual (h,x,P)	0.46882

Chapter 3: Thermo-Physical and Transport Properties of Ethanol-Water Mixtures

3.1 Pure Ethanol

Saturated liquid properties of methanol were calculated using the equations of state found in the REFPROP program [30]. The result was then correlated using polynomials as a function of temperature for use in numerical simulations; the polynomial coefficients are presented in Table 3.7. All properties are in SI units. The polynomial correlations and the NIST outputs were compared over a range of 0-200°C; the error was calculated for 20,000 data points and averaged. The MAE values of the liquid properties are presented in Table 3.8

3.1.1 Liquid Phase

Table 3.1: Polynomial Coefficients for Liquid Density and Specific Heat Capacity

	$f(T)=a1*T^4+a2*T^3+a3*T^2+a4*T+a5$				
$\rho(T)$	a1	a2	a3	a4	a5
$T<78.2$	0.0	-8.873×10^{-6}	-2.567×10^{-4}	-0.8158	806.08
$T\geq78.2$	-1.793×10^{-7}	7.474×10^{-5}	-1.468×10^{-2}	0.2803	775.20
$c_p(T)$					
$T<78.2$	2.707×10^{-6}	-6.118×10^{-4}	3.051×10^{-2}	11.78	2268.83
$T\geq78.2$	8.637×10^{-6}	-3.946×10^{-3}	0.6675	-39.65	3774.52

Table 3.2: MAE Values for Liquid Density and Specific Heat Capacity

Property	MAE (%)
$\rho(T)$	0.00415
$c_p(T)$	0.04024

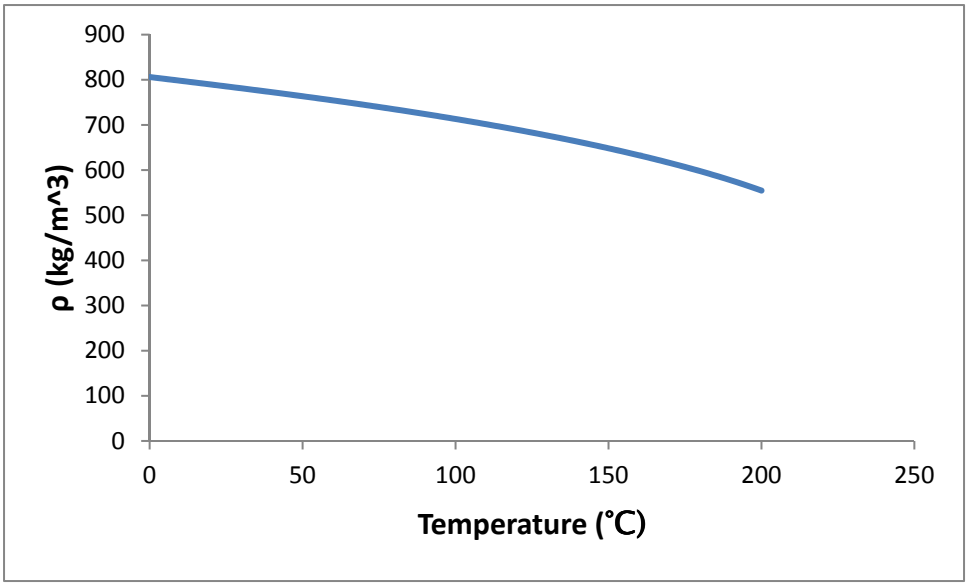

Figure 3.1: Ethanol Liquid Density

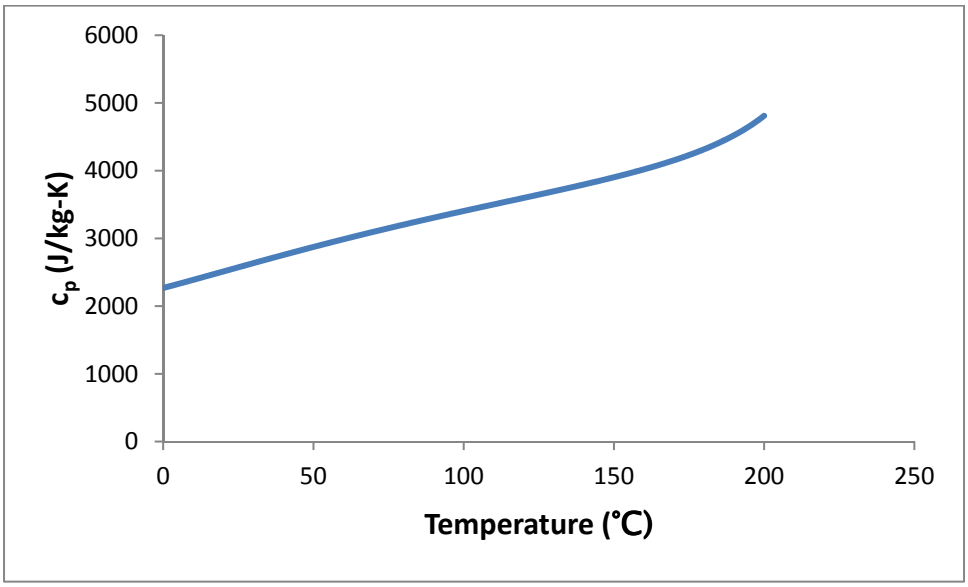

Figure 3.2: Ethanol Liquid Specific Heat Capacity

Table 3.3: Polynomial Coefficients for Liquid Thermal Conductivity and Viscosity

	$f(T)=a1*T^4+a2*T^3+a3*T^2+a4*T+a5$				
k(T)	a1	a2	a3	a4	a5
$T<78.2$	0.0	-3.545×10^{-9}	6.713×10^{-7}	-2.629×10^{-4}	0.1713
$T\geq78.2$	2.826×10^{-11}	-1.313×10^{-8}	2.265×10^{-6}	-3.920×10^{-4}	0.1752
μ(T)					
$T<78.2$	1.398×10^{-11}	-3.931×10^{-9}	5.029×10^{-7}	-3.951×10^{-5}	1.813×10^{-3}
$T\geq78.2$	6.726×10^{-13}	-4.978×10^{-10}	1.467×10^{-7}	-2.157×10^{-5}	1.443×10^{-3}

Table 3.4: MAE Values of Liquid Thermal Conductivity and Viscosity

Property	MAE (%)
k(T)	0.00708
μ(T)	0.05061

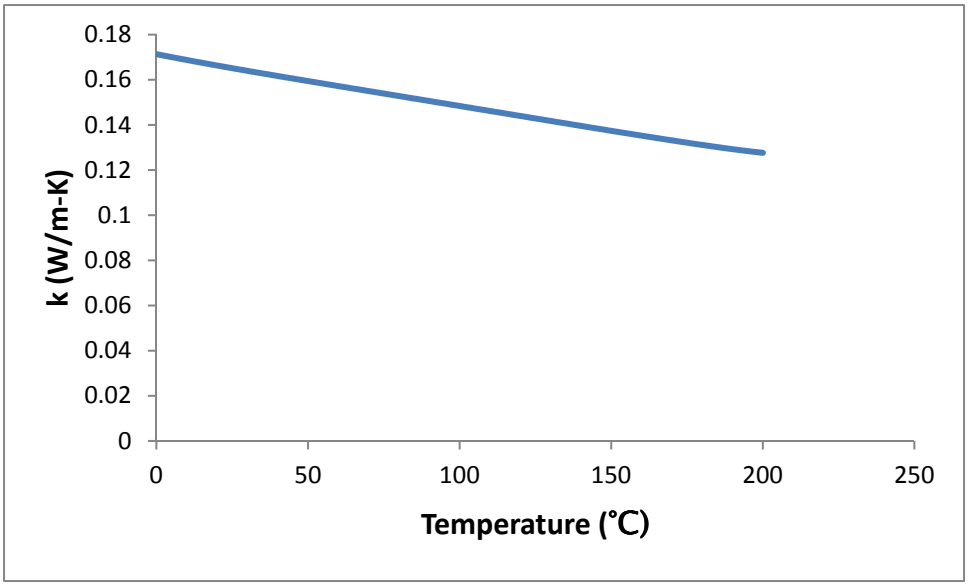

Figure 3.3: Ethanol Liquid Thermal Conductivity

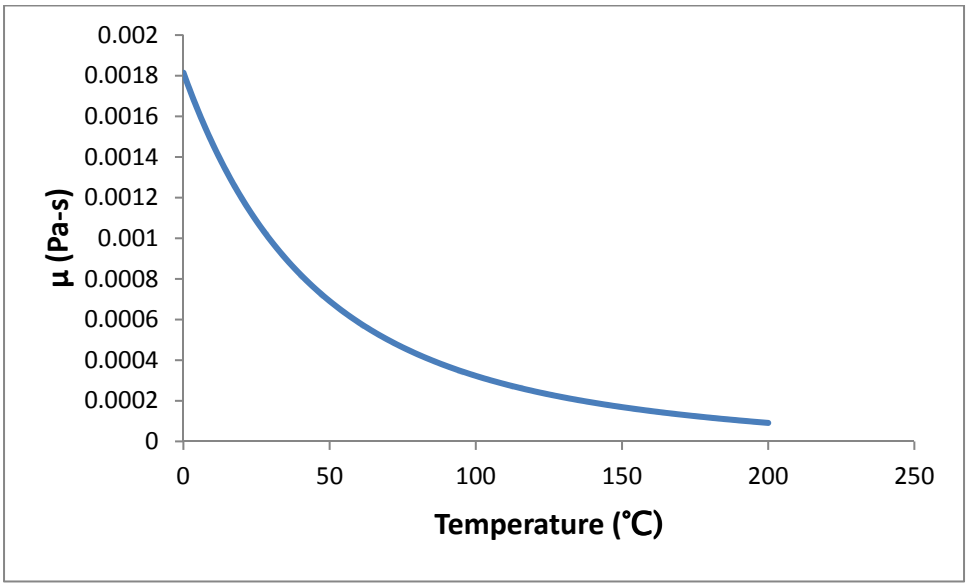

Figure 3.4: Ethanol Liquid Viscosity

Table 3.5: Polynomial Coefficients for Liquid Enthalpy and Surface Tension

	$f(T)=a1*T^4+a2*T^3+a3*T^2+a4*T+a5$				
h(T)	a1	a2	a3	a4	a5
$T<78.2$	0.0	-4.399×10^{-3}	6.473	2260.17	2.000×10^{5}
$T\geq78.2$	0.0	9.685×10^{-3}	1.340	2851.98	1.780×10^{5}
σ(T)					
$T<78.2$	0.0	9.954×10^{-11}	6.917×10^{-8}	-1.308×10^{-4}	2.500×10^{-2}
$T\geq78.2$	0.0	3.609×10^{-10}	-1.190×10^{-8}	-1.222×10^{-4}	2.470×10^{-2}

Table 3.6: MAE Values for Liquid Enthalpy and Surface Tension

Property	MAE (%)
h(T)	0.01301
σ(T)	0.01508

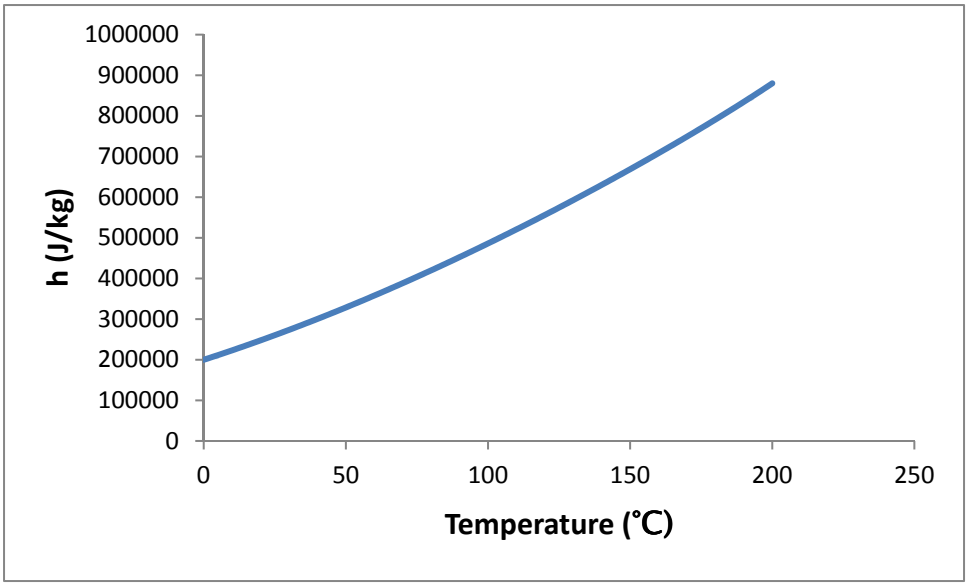

Figure 3.5: Ethanol Liquid Enthalpy

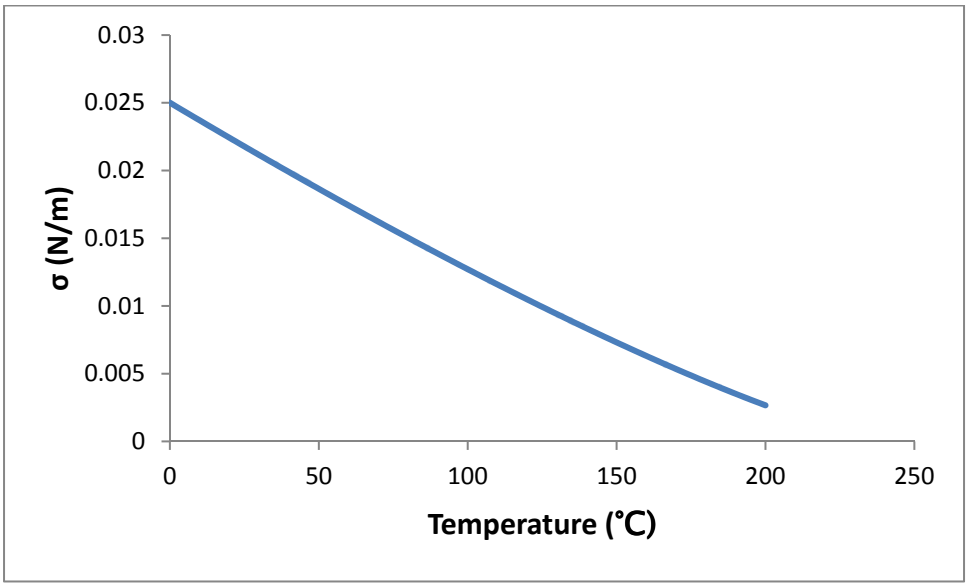

Figure 3.6: Ethanol Liquid Surface Tension

Table 3.7: Summary of Polynomial Curve Fit Coefficients for Liquid Phase Ethanol

	$f(T)=a1*T^4+a2*T^3+a3*T^2+a4*T+a5$				
ρ(T)	a1	a2	a3	a4	a5
T<78.2	0.0	$-8.873x10^{-6}$	$-2.567x10^{-4}$	-0.8158	806.08
T≥78.2	$-1.793x10^{-7}$	$7.474x10^{-5}$	$-1.468x10^{-2}$	0.2803	775.20
$c_p(T)$					
T<78.2	$2.707x10^{-6}$	$-6.118x10^{-4}$	$3.051x10^{-2}$	11.78	2268.83
T≥78.2	$8.637x10^{-6}$	$-3.946x10^{-3}$	0.6675	-39.65	3774.52
k(T)					
T<78.2	0.0	$-3.545x10^{-9}$	$6.713x10^{-7}$	$-2.629x10^{-4}$	0.1713
T≥78.2	$2.826x10^{-11}$	$-1.313x10^{-8}$	$2.265x10^{-6}$	$-3.920x10^{-4}$	0.1752
μ(T)					
T<78.2	$1.398x10^{-11}$	$-3.931x10^{-9}$	$5.029x10^{-7}$	$-3.951x10^{-5}$	$1.813x10^{-3}$
T≥78.2	$6.726x10^{-13}$	$-4.978x10^{-10}$	$1.467x10^{-7}$	$-2.157x10^{-5}$	$1.443x10^{-3}$
h(T)					
T<78.2	0.0	$-4.399x10^{-3}$	6.473	2260.17	$2.000x10^{5}$
T≥78.2	0.0	$9.685x10^{-3}$	1.340	2851.98	$1.780x10^{5}$
σ(T)					
T<78.2	0.0	$9.954x10^{-11}$	$6.917x10^{-8}$	$-1.308x10^{-4}$	$2.500x10^{-2}$
T≥78.2	0.0	$3.609x10^{-10}$	$-1.190x10^{-8}$	$-1.222x10^{-4}$	$2.470x10^{-2}$

Table 3.8: Summary of MAE of the Liquid Phase Ethanol Polynomial Correlations

Property	MAE(%)
ρ(T)	0.00415
$c_p(T)$	0.04024
k(T)	0.00708
μ(T)	0.05061
h(T)	0.01301
σ(T)	0.01508

3.1.2 Vapor Phase

Table 3.9: Polynomial Coefficients for Vapor Density and Specific Heat Capacity

	$f(T)=a1*T^4+a2*T^3+a3*T^2+a4*T+a5$				
$\rho_g(T)$	a1	a2	a3	a4	a5
$T<78.2$	$2.124x10^{-8}$	$2.881x10^{-7}$	$8.621x10^{-5}$	$1.939x10^{-3}$	$3.350x10^{-2}$
$T\geq78.2$	$1.403x10^{-7}$	$-5.276x10^{-5}$	$9.098x10^{-3}$	$-6.798x10^{-1}$	19.23
$c_{pg}(T)$					
$T<78.2$	$5.679x10^{-7}$	$3.313x10^{-5}$	$2.746x10^{-3}$	2.912	1524.35
$T\geq78.2$	$1.127x10^{-5}$	$-5.147x10^{-3}$	0.9273	-69.21	3596.60

Table 3.10: MAE Values for Vapor Density and Specific Heat Capacity

Property	MAE (%)
$\rho_g(T)$	0.27945
$c_{pg}(T)$	0.08159

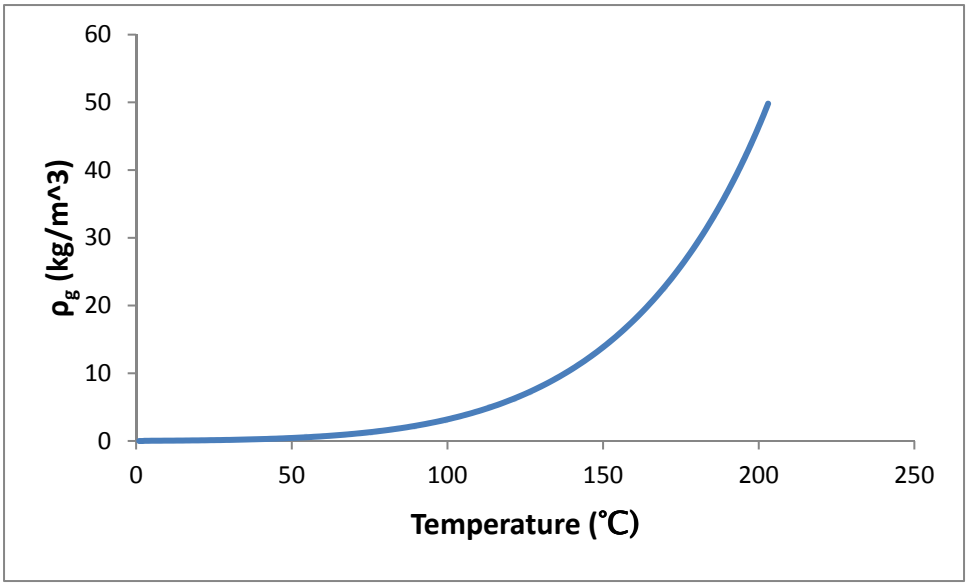

Figure 3.7: Ethanol Vapor Density

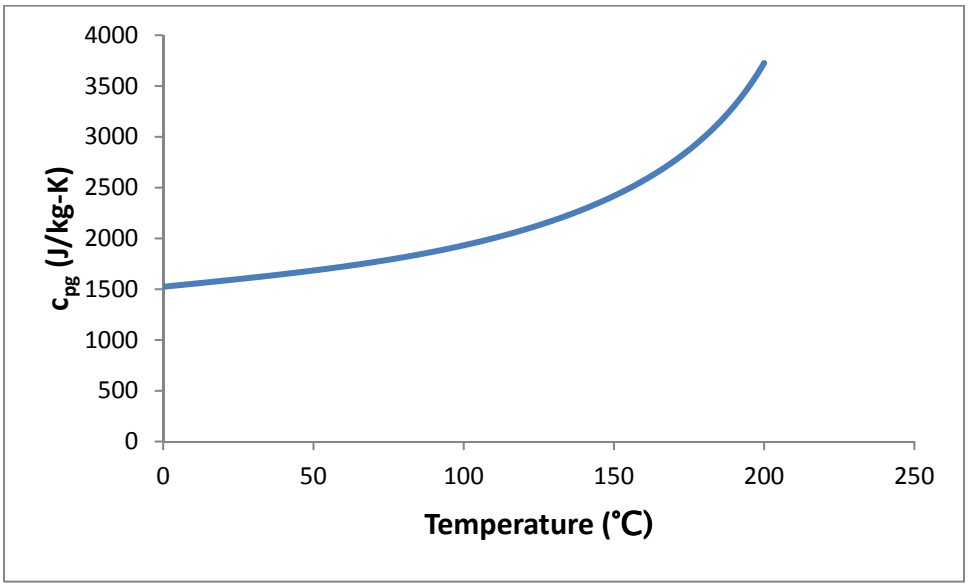

Figure 3.8: Ethanol Vapor Specific Heat Capacity

Table 3.11: Polynomial Coefficients for Vapor Thermal Conductivity and Viscosity

	$f(T)=a1*T^4+a2*T^3+a3*T^2+a4*T+a5$				
$k_g(T)$	a1	a2	a3	a4	a5
$T<78.2$	0.0	$7.100x10^{-10}$	$1.334x10^{-7}$	$5.926x10^{-5}$	$1.620x10^{-2}$
$T\geq78.2$	$9.271x10^{-11}$	$-3.922x10^{-8}$	$6.827x10^{-6}$	$-4.444x10^{-4}$	$3.034x10^{-2}$
$\mu_g(T)$					
$T<78.2$	$-1.215x10^{-16}$	$-1.382x10^{-13}$	$-1.626x10^{-12}$	$3.139x10^{-8}$	$8.839x10^{-6}$
$T\geq78.2$	$1.495x10^{-14}$	$-6.613x10^{-12}$	$1.040x10^{-9}$	$-4.200x10^{-8}$	$1.073x10^{-5}$

Table 3.12: MAE Values for Vapor Thermal Conductivity and Viscosity

Property	MAE (%)
$k_g(T)$	0.03803
$\mu_g(T)$	0.01096

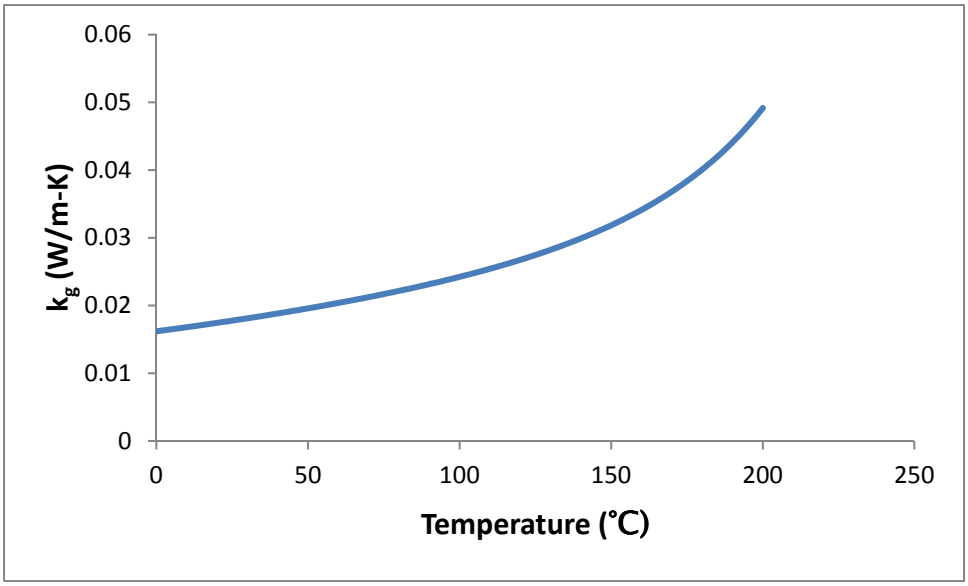

Figure 3.9: Ethanol Vapor Thermal Conductivity

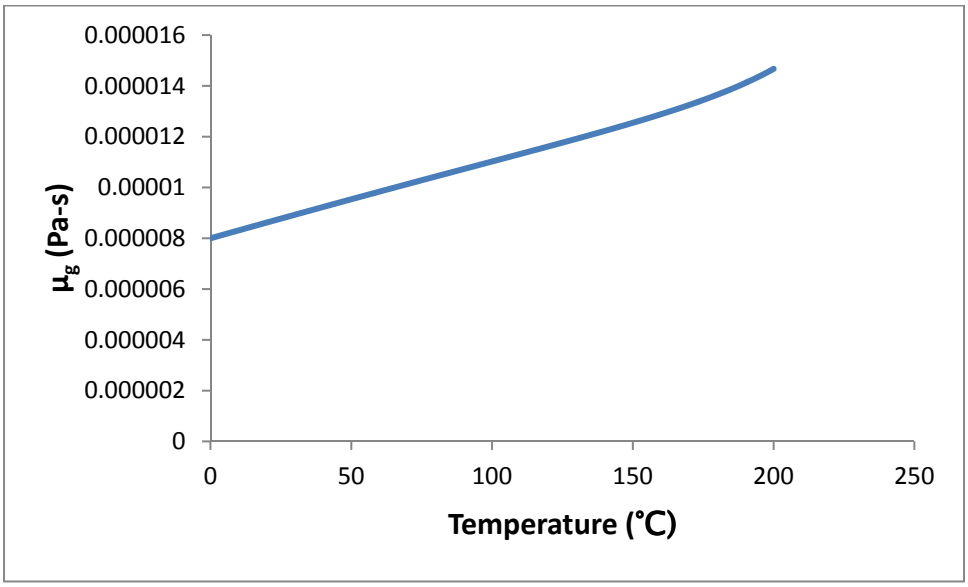

Figure 3.10: Ethanol Vapor Viscosity

Table 3.13: Polynomial Coefficients for Vapor Enthalpy and Saturation Pressure

	$f(T)=a1*T^4+a2*T^3+a3*T^2+a4*T+a5$				
$h_g(T)$	a1	a2	a3	a4	a5
$T<78.2$	0.0	0.0	$-1.045x10^{-11}$	$3.125x10^{-8}$	$7.998x10^{-6}$
$T\geq78.2$	$9.768x10^{-15}$	$-4.337x10^{-12}$	$7.272x10^{-10}$	$-2.469x10^{-8}$	$9.577x10^{-6}$
Psat(T)					
$T<78.2$	$1.589x10^{-3}$	$1.717x10^{-4}$	5.336	93.61	1668.67
$T\geq78.2$	0.0	1.014	-206.88	$1.862x10^{4}$	$-5.798x10^{5}$

Table 3.14: MAE Values for Vapor Enthalpy and Saturation Pressure

Property	MAE (%)
$h_g(T)$	0.00527
Psat(T)	0.30414

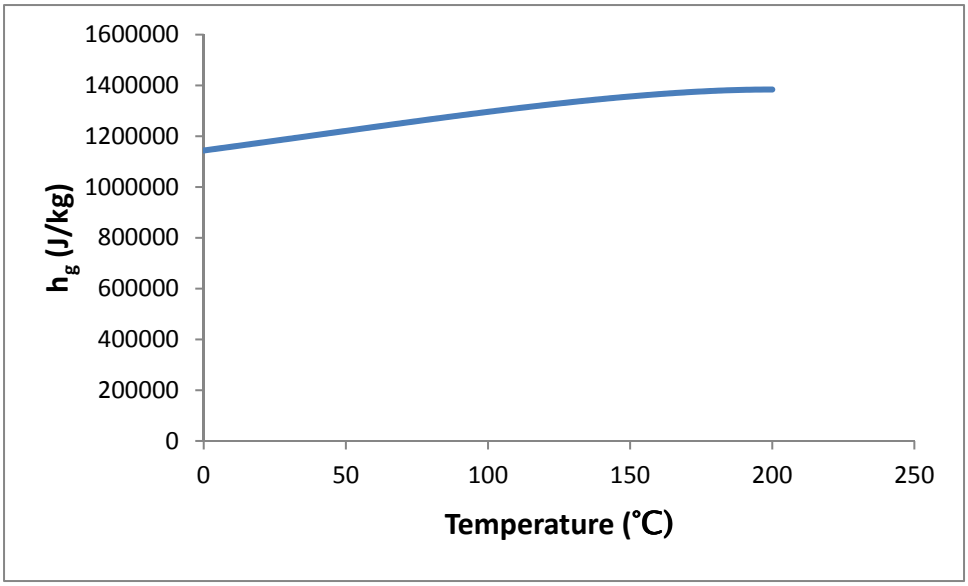

Figure 3.11: Ethanol Vapor Enthalpy

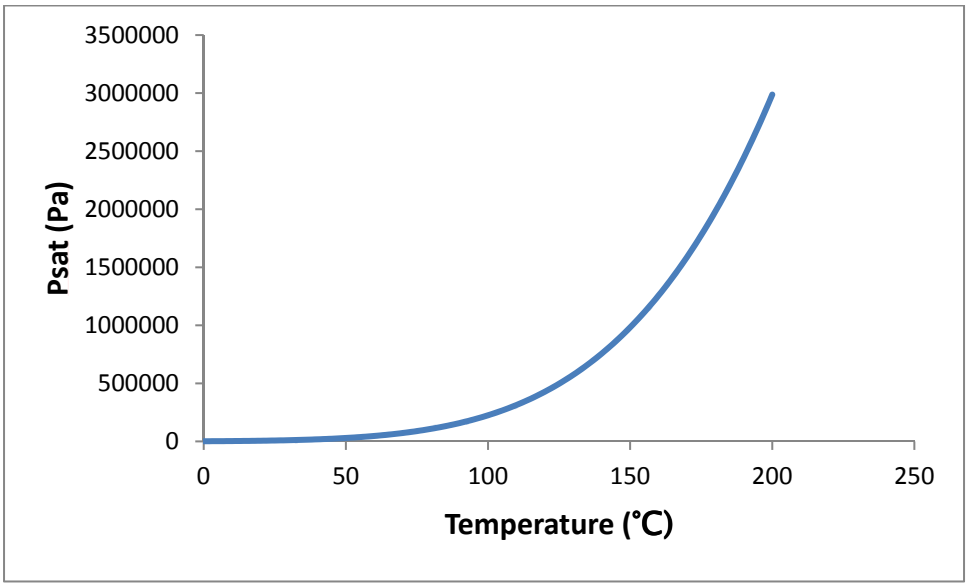

Figure 3.12: Ethanol Saturation Pressure

Table 3.15: Summary of Polynomial Curve Fit Coefficients for Vapor Phase Ethanol

	$f(T)=a1*T^4+a2*T^3+a3*T^2+a4*T+a5$				
$\rho_g(T)$	a1	a2	a3	a4	a5
T<78.2	$2.124x10^{-8}$	$2.881x10^{-7}$	$8.621x10^{-5}$	$1.939x10^{-3}$	$3.350x10^{-2}$
T≥78.2	$1.403x10^{-7}$	$-5.276x10^{-5}$	$9.098x10^{-3}$	$-6.798x10^{-1}$	19.23
$c_{pg}(T)$					
T<78.2	$5.679x10^{-7}$	$3.313x10^{-5}$	$2.746x10^{-3}$	2.912	1524.35
T≥78.2	$1.127x10^{-5}$	$-5.147x10^{-3}$	0.9273	-69.21	3596.60
$k_g(T)$					
T<78.2	0.0	$7.100x10^{-10}$	$1.334x10^{-7}$	$5.926x10^{-5}$	$1.620x10^{-2}$
T≥78.2	$9.271x10^{-11}$	$-3.922x10^{-8}$	$6.827x10^{-6}$	$-4.444x10^{-4}$	$3.034x10^{-2}$
$\mu_g(T)$					
T<78.2	$-1.215x10^{-16}$	$-1.382x10^{-13}$	$-1.626x10^{-12}$	$3.139x10^{-8}$	$8.839x10^{-6}$
T≥78.2	$1.495x10^{-14}$	$-6.613x10^{-12}$	$1.040x10^{-9}$	$-4.200x10^{-8}$	$1.073x10^{-5}$
$h_g(T)$					
T<78.2	0.0	0.0	$-1.045x10^{-11}$	$3.125x10^{-8}$	$7.998x10^{-6}$
T≥78.2	$9.768x10^{-15}$	$-4.337x10^{-12}$	$7.272x10^{-10}$	$-2.469x10^{-8}$	$9.577x10^{-6}$
Psat(T)					
T<78.2	$1.589x10^{-3}$	$1.717x10^{-4}$	5.336	93.61	1668.67
T≥78.2	0.0	1.014	-206.88	$1.862x10^{4}$	$-5.798x10^{5}$

Table 3.16: Summary of MAE of the Vapor Phase Ethanol Polynomial Correlations

Property	MAE(%)
$\rho_g(T)$	0.27945
$c_{pg}(T)$	0.08159
$k_g(T)$	0.03803
$\mu_g(T)$	0.01096
$h_g(T)$	0.00527
Psat(T)	0.30414

3.2 Ethanol-Water Mixtures

Some properties of ethanol-water mixtures are not adequately described by available mixing rules. For property routines whose MAE values were over 8% a curve fitting approach was used in order to achieve a better agreement with the REFPROP data. This limit is based on the reported uncertainty for the liquid and vapor thermal conductivity mixing rules.

3.2.1 Liquid Phase

Table 3.17: Summary of Liquid Phase Mixing Rules

Property	Source	Correlation	Uncertainty
ρ_f(T,x)	[20]	$\frac{1}{\rho_m} = \sum_{i=1}^{2} \frac{x_i}{\rho_i}$	2.409%
σ(T,x)	[20]	$\sigma_m = \sum_{i=1}^{2} w_i \sigma_i$	8.264%
c_{pf}(T,x)		Polynomial Correlation	1.439%
h_f(T,x)	[20]	$h_m = \sum_{i=1}^{2} x_i h_i$	4.414%
μ_f(T,x)	[26]	$\mu_m = \frac{\mu_g^c}{1+\varphi_{c,aw}\left[\frac{x_g^{aw}}{x_g^c}\right]} + \frac{\mu_g^{aw}}{1+\varphi_{aw,c}\left[\frac{x_g^c}{x_g^{aw}}\right]}$ $\varphi_{c,aw} = \frac{\left[1+\left(\mu_g^c/\mu_g^{aw}\right)^{\frac{1}{2}}(M_{wt}^{aw}/M_{wt}^c)^4\right]^2}{[8(1+M_{wt}^c/M_{wt}^{aw})]^{\frac{1}{2}}}$ $\varphi_{aw,c} = \frac{\left[1+\left(\mu_g^{aw}/\mu_g^c\right)^{\frac{1}{2}}(M_{wt}^{aw}/M_{wt}^c)^4\right]^2}{[8(1+M_{wt}^{aw}/M_{wt}^c)]^{\frac{1}{2}}}$	7.906%
k_f(T,x)	[20]	$k_m = \sum_{i=1}^{2}\sum_{j=1}^{2} \Phi_i \Phi_j \frac{2k_i k_j}{k_i + k_j}$	4-8%

Again, the Li correlation [20], as shown in the previous table, was used to calculate vapor mixture density. This time an MAE value of 2.409% was achieved using this correlation with a mass basis. While a linear mixing rule adequately described mixture properties for a methanol-water mixture, it will be seen that ethanol-water mixtures are not linear functions of mixture composition.

The following figure shows the liquid mixture surface tension as obtained from the REFPROP program. An MAE value of 8.264% was achieved with a linear mass based mixing rule. This MAE value was considered acceptable, but may be improved.

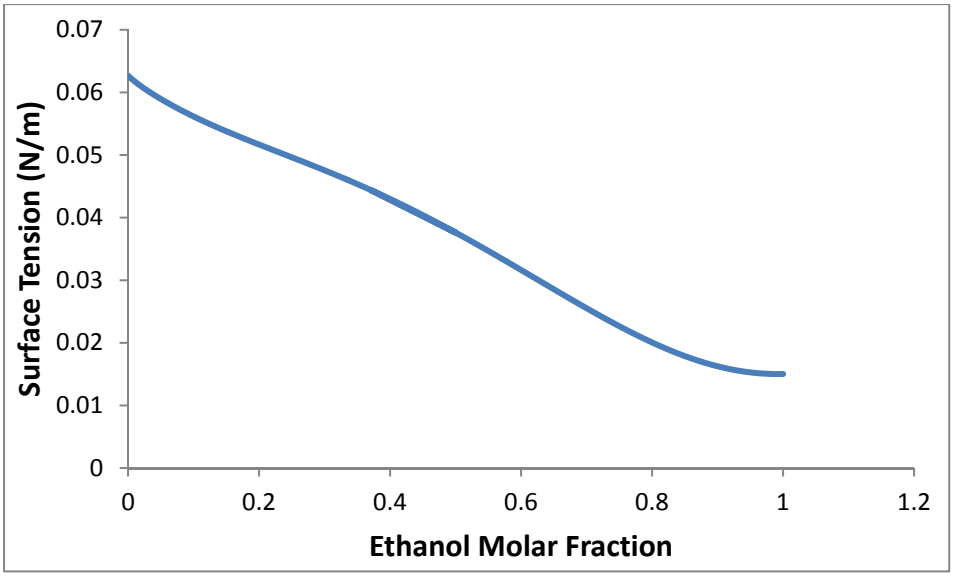

Figure 3.13: Liquid Mixture Surface Tension

Liquid mixture specific heat capacity when calculated with a linear rule has an MAE value of over 10% which is higher than the 8% limit imposed in this study. The 8% limit is based on the reported uncertainties for the liquid and vapor thermal conductivity mixing rules. Because of the higher error, a polynomial curve was instead fit to the REFPROP output. The average error was reduced to 1.439%. The coefficients of the correlation can be found on the following page.

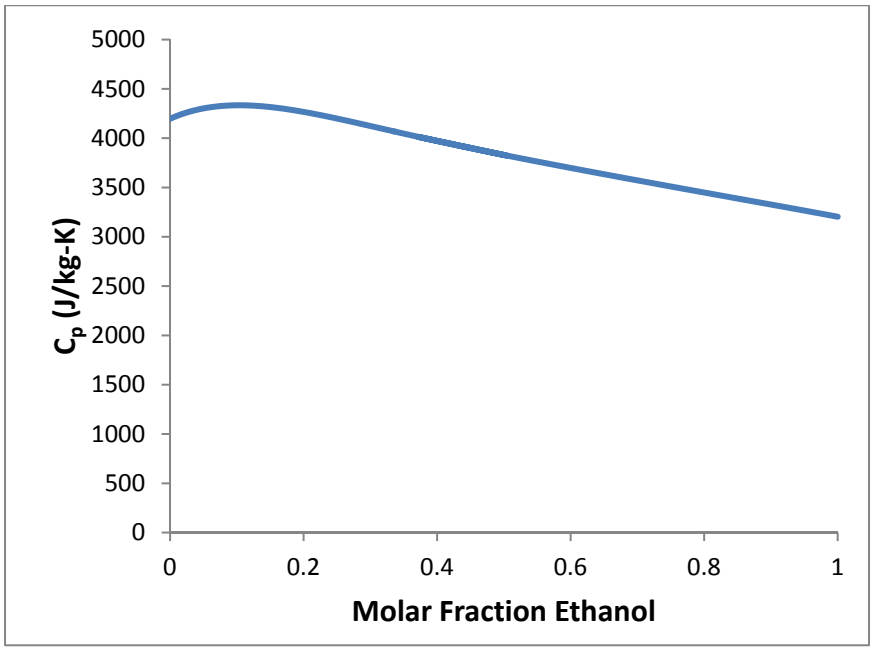

Figure 3.14: Liquid Mixture Specific Heat Capacity

Table 3.18: Polynomial Curve Fit Coefficients for Liquid Phase Specific Heat

	$f(x)=a1*x^6+a2*x^5+a3*x^4+a4*x^3+a5*x^2+a6*x+a7$						
$c_{pf}(T,x)$	a1	a2	a3	a4	a5	a6	a7
T = 0°C	$-1.216x10^4$	$4.439x10^4$	$-6.402x10^4$	$4.861x10^4$	$-1.858x10^4$	$8.358x10^2$	$4.247x10^3$

		$f(T)=b1*t^6+b2*t^5+b3*t^4+b4*t^3+b5*t^2+b6*t+b7$						
		b1	b2	b3	b4	b5	b6	b7
T < 200°C	a1	0.0	$-8.543x10^{-7}$	$4.094x10^{-4}$	$-6.282x10^{-2}$	2.808	$4.154x10^1$	$-1.216x10^4$
	a2	0.0	$3.400x10^{-6}$	$-1.733x10^{-3}$	$3.011x10^{-1}$	$-1.959x10^1$	$2.886x10^2$	$4.439x10^4$
	a3	$6.811x10^{-8}$	$-4.629x10^{-5}$	$1.213x10^{-2}$	-1.516	$8.924x10^1$	$-1.919x10^3$	$-6.402x10^4$
	a4	$-4.781x10^{-8}$	$3.305x10^{-5}$	$-8.912x10^{-3}$	1.172	$-7.578x10^1$	$1.940x10^3$	$4.861x10^4$
	a5	$1.670x10^{-8}$	$-1.177x10^{-5}$	$3.277x10^{-3}$	$-4.537x10^{-1}$	$3.202x10^1$	$-9.436x10^2$	$-1.858x10^4$
	a6	$-2.326x10^{-9}$	$1.687x10^{-6}$	$-4.875x10^{-4}$	$7.138x10^{-2}$	-5.536	$2.023x10^2$	$8.358x10^2$
	a7	$4.625x10^{-11}$	$-3.295x10^{-8}$	$9.462x10^{-6}$	$-1.351x10^{-3}$	$1.099x10^{-1}$	-4.422	$4.247x10^3$

For liquid mixture viscosity, there were an inadequate number of experimental data points to implement the Lobe correlation over the desired temperature range. Works dealing with liquid ethanol-water viscosity were very old and limited in scope [31]. It was thought that the modified Wilke method used for methanol-water vapor viscosity, which gave a similarly shaped curve as the Lobe correlation, could also be used for liquid mixture viscosity. Initially, this approach resulted in a 21% error, but by changing the exponent in the interaction parameter from 0.25 to 4 the MAE value was able to be reduced to 8%. The following figure shows the Wilke method curve against the experimental data for ethanol-water liquid viscosity at 50°C [23]. As seen in Figure 2.20, the mixture viscosity curve flattens with increasing temperature; this is also the case for ethanol-water mixtures [18]. The modified correlation is able to capture this trend.

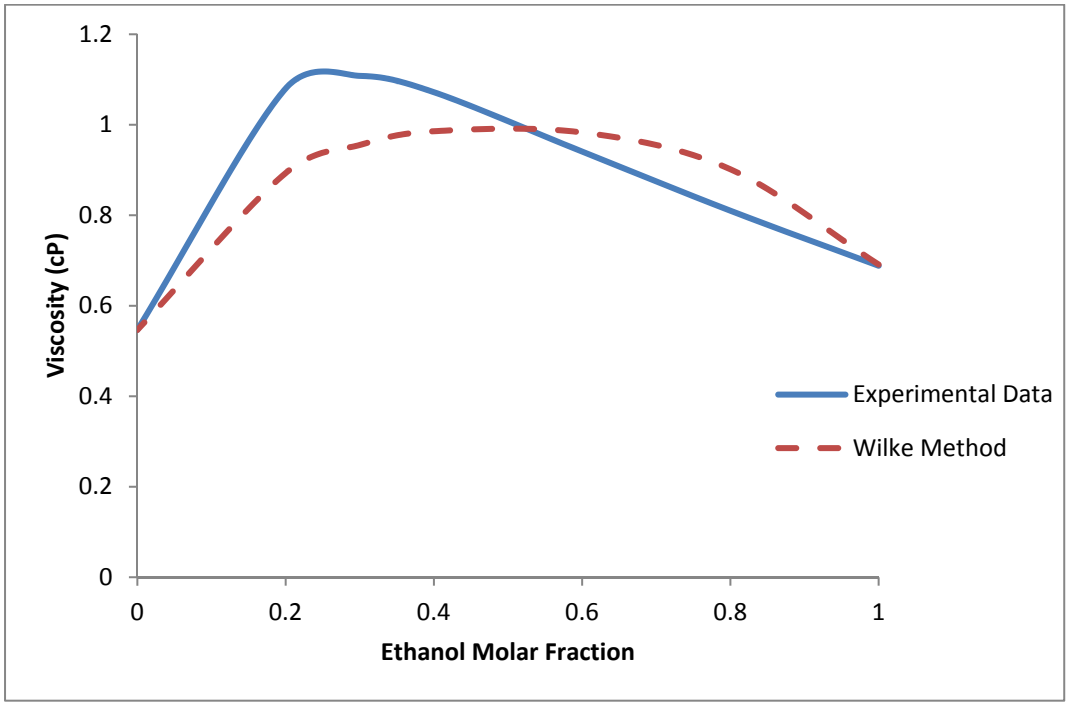

Figure 3.15: Wilke Method Correlation Against Experimental Data

3.2.1 Vapor Phase

Table 3.19: Summary of Vapor Phase Mixing Rules

Property	Source	Correlation	Uncertainty
ρ_g(T,x)		Polynomial Correlation	0.475%
c_{pg}(T,x)	[20]	$c_{pm} = \sum_{i=1}^{2} x_i c_{pi}$	3.055%
h_g(T,x)	[20]	$h_m = \sum_{i=1}^{2} w_i h_i$	0.037%
μ_g(T,x)	[26]	$\mu_m = \frac{\mu_g^c}{1+\varphi_{c,aw}\left[\frac{x_g^{aw}}{x_g^c}\right]} + \frac{\mu_g^{aw}}{1+\varphi_{aw,c}\left[\frac{x_g^c}{x_g^{aw}}\right]}$ $\varphi_{c,aw} = \frac{\left[1+\left(\mu_g^c/\mu_g^{aw}\right)^{\frac{1}{2}}(M_{wt}^{aw}/M_{wt}^c)^{\frac{1}{4}}\right]^2}{[8(1+M_{wt}^c/M_{wt}^{aw})]^{\frac{1}{2}}}$ $\varphi_{aw,c} = \frac{\left[1+\left(\mu_g^{aw}/\mu_g^c\right)^{\frac{1}{2}}(M_{wt}^{aw}/M_{wt}^c)^{\frac{1}{4}}\right]^2}{[8(1+M_{wt}^{aw}/M_{wt}^c)]^{\frac{1}{2}}}$	2-4%
k_g(T,x)	[27]	$k_m = \sum_{i=1}^{n} \frac{x_i k_i}{\sum_{j=1}^{n} x_j \varphi_{ij}}$	5-8%

The Li correlation previously used for vapor mixture density fails to adequately describe the behavior of ethanol-water density yielding an average error of 14.48%. A polynomial curve was fitted to the REFPROP output and the MAE value was reduced to 0.475%. The coefficients are presented in the following table.

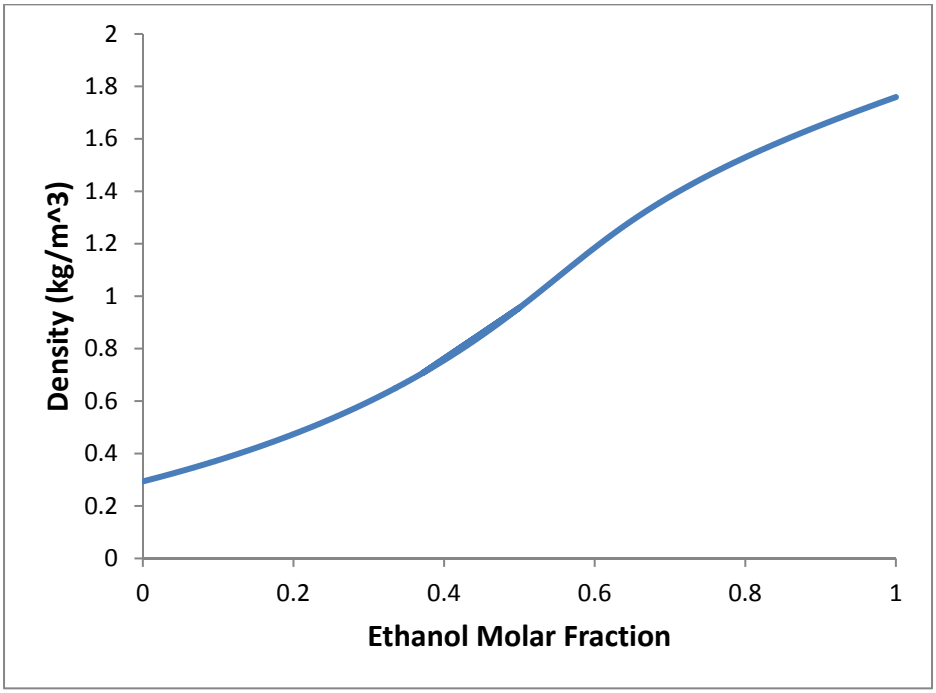

Figure 3.16: Vapor Mixture Density

Table 3.20: Polynomial Curve Fit Coefficients for Vapor Phase Mixture Density

		$f(x)=a1*x^6+a2*x^5+a3*x^4+a4*x^3+a5*x^2+a6*x+a7$						
$\rho_g(T,x)$	a1	a2	a3	a4	a5	a6	a7	
T = 0°C	$4.014x10^{-01}$	-1.023	$8.856x10^{-01}$	$-2.963x10^{-01}$	$6.107x10^{-02}$	$9.841x10^{-03}$	$5.058x10^{-03}$	
		$f(T)=b1*t6+b2*t5+b3*t4+b4*t3+b5*t2+b6*t+b7$						
		b1	b2	b3	b4	b5	b6	b7
T < 200°C	a1	$6.353x10^{-12}$	$-2.251x10^{-09}$	$1.740x10^{-07}$	$5.192x10^{-06}$	$8.048x10^{-04}$	$2.426x10^{-02}$	$4.014x10^{-01}$
	a2	$-3.555x10^{-12}$	$-5.978x10^{-10}$	$8.640x10^{-07}$	$-1.160x10^{-04}$	$1.904x10^{-03}$	$-1.195x10^{-01}$	-1.023
	a3	$-1.564x10^{-11}$	$9.731x10^{-09}$	$-2.634x10^{-06}$	$2.457x10^{-04}$	$-7.162x10^{-03}$	$1.815x10^{-01}$	$8.856x10^{-01}$
	a4	$1.898x10^{-11}$	$-1.001x10^{-08}$	$2.240x10^{-06}$	$-1.860x10^{-04}$	$6.305x10^{-03}$	$-1.158x10^{-01}$	$-2.963x10^{-01}$
	a5	$-5.140x10^{-12}$	$2.703x10^{-09}$	$-5.684x10^{-07}$	$4.562x10^{-05}$	$-1.566x10^{-03}$	$2.720x10^{-02}$	$6.107x10^{-02}$
	a6	$7.305x10^{-13}$	$-3.337x10^{-10}$	$7.575x10^{-08}$	$-5.056x10^{-06}$	$2.242x10^{-04}$	$-2.124x10^{-03}$	$9.841x10^{-03}$
	a7	$4.649x10^{-15}$	$4.386x10^{-12}$	$3.080x10^{-09}$	$4.946x10^{-08}$	$1.485x10^{-05}$	$2.747x10^{-04}$	$5.058x10^{-03}$

Here, the equations for vapor mixture viscosity and thermal conductivity are the same as the ones used for methanol-water mixtures. However, due to the difference in mixture components, the shapes of the curves are slightly different and are presented in the following figures.

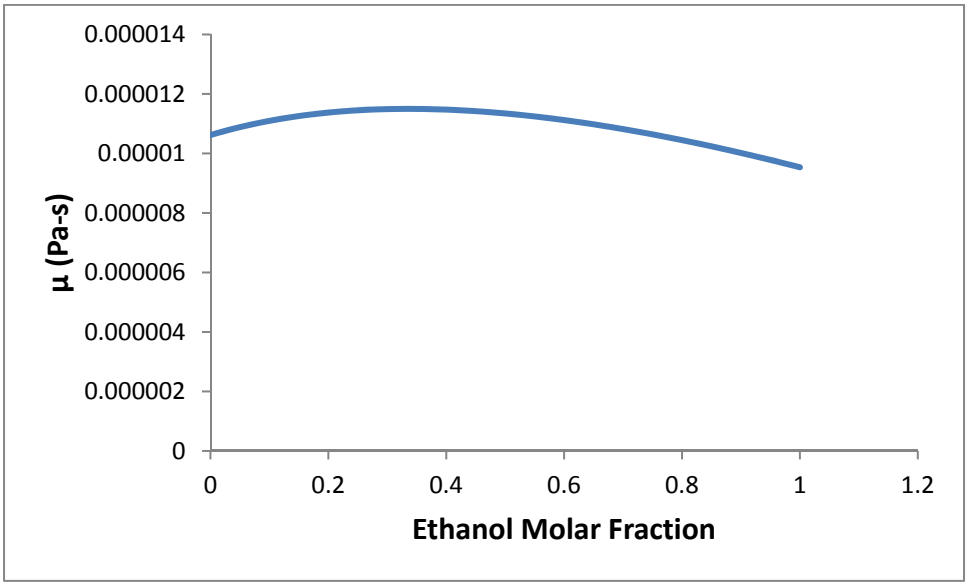

Figure 3.17: Vapor Mixture Viscosity

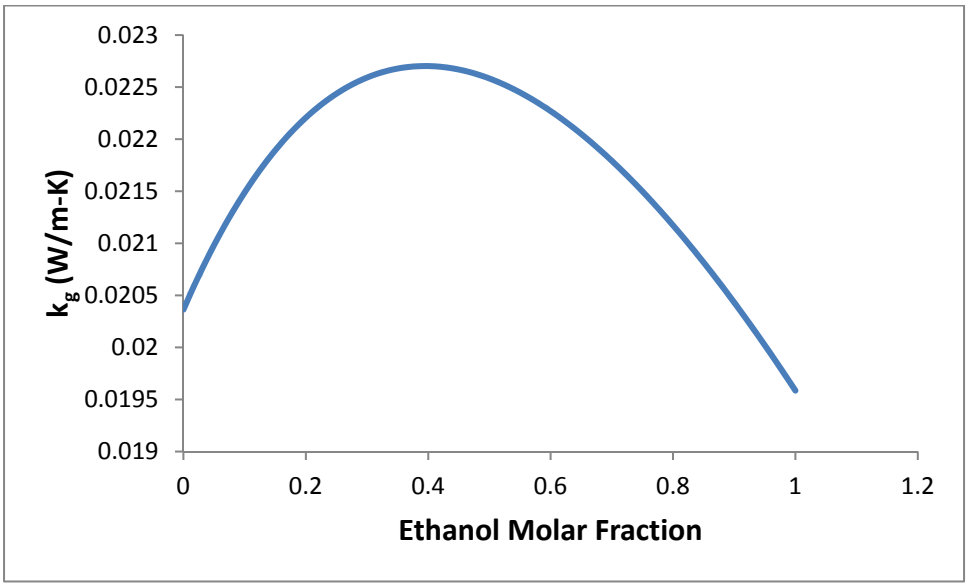

Figure 3.18: Vapor Mixture Thermal Conductivity

3.2.3 Phase Diagram Properties

Unlike methanol-water mixtures, ethanol and water form an azeotrope. Around a molar fraction of 0.92, the mixture acts as a pure substance; the vapor and liquid saturation temperature is the same. However, the temperature difference between the azeotropic point and pure ethanol is extremely small going from 77.86 to 77.9°C or a 0.05% change.

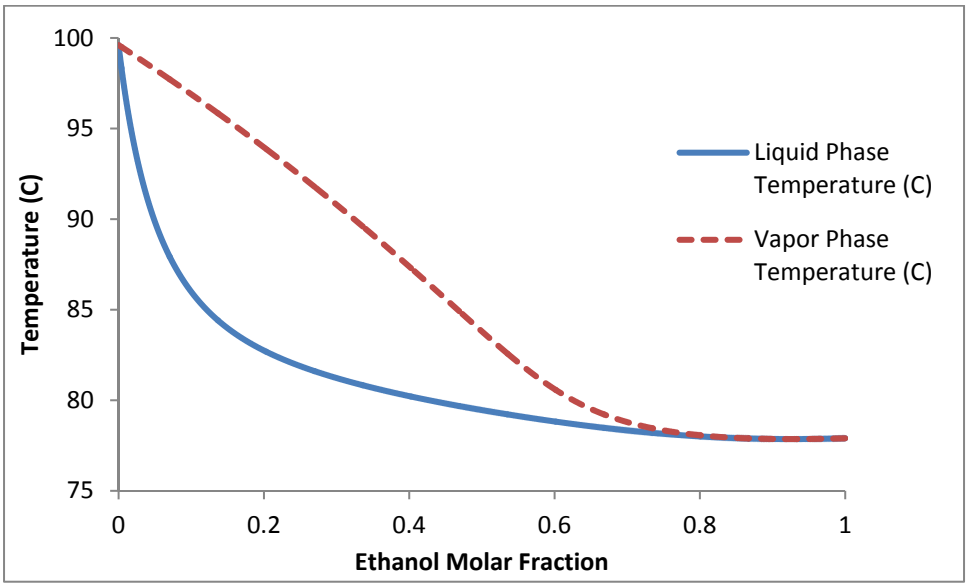

Figure 3.19: Phase Diagram for Binary Ethanol/Water Mixture at 1 bar

Table 3.21: Polynomial Curve Fit Coefficients for Liquid Phase Saturation Temperature

	$f(x)=a1*x^6+a2*x^5+a3*x^4+a4*x^3+a5*x^2+a6*x+a7$						
$Tsat_f(x,P)$	a1	a2	a3	a4	a5	a6	a7
P = 1 bar	888.0	-3042	4125	-2815	1022	-197.5	97.99

		$f(P)=b1*P^3+b2*P^2+b3*P+b4$			
		b1	b2	b3	b4
P < 3 bar	a1	7.902	-66.24	187.4	759.4
	a2	-26.40	221.6	-632.8	-2605
	a3	34.53	-290.8	842.0	3541
	a4	-22.34	189.0	-560.6	-2422
	a5	7.462	-63.75	198.7	879.5
	a6	-1.263	11.05	-38.65	-168.7
	a7	1.184	-10.72	44.45	63.14

Table 3.22: Polynomial Curve Fit Coefficients for Vapor Phase Saturation Temperature

	$f(x)=a1*x^6+a2*x^5+a3*x^4+a4*x^3+a5*x^2+a6*x+a7$						
$Tsat_g(x,P)$	a1	a2	a3	a4	a5	a6	a7
P = 1 bar	-2.726	-174.6	416.0	-297.4	70.62	-34.01	99.77

		$f(P)=b1*P^3+b2*P^2+b3*P+b4$			
		b1	b2	b3	b4
P < 3 bar	a1	2.920	-27.31	114.3	-92.53
	a2	-10.05	92.68	-373.7	116.0
	a3	12.59	-114.6	444.2	74.40
	a4	-6.777	60.85	-225.6	-126.4
	a5	1.510	-13.38	47.64	34.93
	a6	-0.3105	2.793	-11.19	-25.32
	a7	1.203	-10.87	44.80	64.70

Table 3.23: MAE Values for Saturation Temperature Routines

Property	MAE (%)
$Tsat_f(x,P)$	0.150819
$Tsat_g(x,P)$	0.078516

3.2.4 Quality

Table 3.24: Polynomial Curve Fit Coefficients for Mixture Quality

Qual(h,x,P)	$f(h)=a1*h^3+a2*h^2+a3*h+a4$
a1	$f(x)=b1*x^5+b2*x^4+b3*x^3+b4*x^2+b5*x+b6$
a2	$f(x)=c1*x^5+c2*x^4+c3*x^3+c4*x^2+c5*x+c6$
a3	$f(x)=d1*x^5+d2*x^4+d3*x^3+d4*x^2+d5*x+d6$
a4	$f(x)=e1*x^5+e2*x^4+e3*x^3+e4*x^2+e5*x+e6$

	$f(P)=f1*P^4+f2*P^3+f3*P^2+f4*P+f5$				
	e1	e2	e3	e4	e5
b1	$-3.679*10^{-16}$	$2.999*10^{-15}$	$-8.758*10^{-15}$	$1.081*10^{-14}$	$7.169*10^{-15}$
b2	$5.518*10^{-16}$	$-4.498*10^{-15}$	$1.314*10^{-14}$	$-1.622*10^{-14}$	$7.169*10^{-15}$
b3	$-3.127*10^{-16}$	$2.549*10^{-15}$	$-7.447*10^{-15}$	$9.197*10^{-15}$	$-4.071*10^{-15}$
b4	$8.280*10^{-17}$	$-6.750*10^{-16}$	$1.972*10^{-15}$	$-2.438*10^{-15}$	$1.076*10^{-15}$
b5	$-1.009*10^{-17}$	$8.224*10^{-17}$	$-2.404*10^{-16}$	$2.972*10^{-16}$	$-1.305*10^{-16}$
b6	$4.418*10^{-19}$	$-3.602*10^{-18}$	$1.053*10^{-17}$	$-1.302*10^{-17}$	$5.729*10^{-18}$
c1	$-3.278*10^{-10}$	$2.212*10^{-09}$	$-4.913*10^{-09}$	$4.204*10^{-09}$	$-1.111*10^{-09}$
c2	$4.563*10^{-10}$	$-2.822*10^{-09}$	$5.224*10^{-09}$	$-2.817*10^{-09}$	$-1.319*10^{-10}$
c3	$-1.904*10^{-10}$	$9.046*10^{-10}$	$-4.626*10^{-10}$	$-2.054*10^{-09}$	$1.820*10^{-09}$
c4	$1.968*10^{-11}$	$5.190*10^{-11}$	$-8.662*10^{-10}$	$1.932*10^{-09}$	$-1.117*10^{-09}$
c5	$2.334*10^{-12}$	$-4.981*10^{-11}$	$2.492*10^{-10}$	$-4.329*10^{-10}$	$2.240*10^{-10}$
c6	$-2.954*10^{-13}$	$3.932*10^{-12}$	$-1.661*10^{-11}$	$2.669*10^{-11}$	$-1.343*10^{-11}$
d1	$-2.467*10^{-04}$	$2.003*10^{-03}$	$-5.825*10^{-03}$	$7.181*10^{-03}$	$-3.069*10^{-03}$
d2	$5.960*10^{-04}$	$-4.839*10^{-03}$	$1.408*10^{-02}$	$-1.737*10^{-02}$	$7.390*10^{-03}$
d3	$-5.173*10^{-04}$	$4.201*10^{-03}$	$-1.223*10^{-02}$	$1.509*10^{-02}$	$-6.381*10^{-03}$
d4	$1.954*10^{-04}$	$-1.587*10^{-03}$	$4.619*10^{-03}$	$-5.707*10^{-03}$	$2.391*10^{-03}$
d5	$-3.129*10^{-05}$	$2.542*10^{-04}$	$-7.402*10^{-04}$	$9.152*10^{-04}$	$-3.783*10^{-04}$
d6	$1.646*10^{-06}$	$-1.337*10^{-05}$	$3.891*10^{-05}$	$-4.804*10^{-05}$	$2.046*10^{-05}$
e1	$6.873*10^{+01}$	$-5.567*10^{+02}$	$1.615*10^{+03}$	$-1.990*10^{+03}$	$8.527*10^{+02}$
e2	$-1.663*10^{+02}$	$1.347*10^{+03}$	$-3.911*10^{+03}$	$4.823*10^{+03}$	$-2.059*10^{+03}$
e3	$1.445*10^{+02}$	$-1.171*10^{+03}$	$3.401*10^{+03}$	$-4.199*10^{+03}$	$1.784*10^{+03}$
e4	$-5.460*10^{+01}$	$4.426*10^{+02}$	$-1.286*10^{+03}$	$1.591*10^{+03}$	$-6.703*10^{+02}$
e5	8.746	$-7.091*10^{+01}$	$2.062*10^{+02}$	$-2.557*10^{+02}$	$1.063*10^{+02}$
e6	$-4.589*10^{-01}$	3.718	$-1.079*10^{+01}$	$1.328*10^{+01}$	-5.692

Again, quality was correlated as a function of mixture enthalpy, initial composition, and pressure. Quality is a 3rd order polynomial function of enthalpy. Each of the four coefficients (series a) are 5th order polynomial functions of mixture composition. The final 24 coefficients (series b, c, d, and e) are each 4th order polynomial functions of pressure. The subroutine is able to achieve a fair level of agreement with the REFPROP output, but it is not able to achieve the same level of accuracy as the quality routine for methanol-water mixtures. The MAE value is presented in the following table.

Table 3.25: MAE Value for Quality Subroutine

Property	MAE (%)
Qual (h,x,P)	7.06593

Chapter 4: Single Phase Numerical Modeling

The effectiveness of the new methanol-water mixture property correlations was verified using numerical simulation. Results from the simulation were then compared against previously attained experimental data.

4.1 Simulation Setup

In the present study, a three-dimensional finite volume based simulation was conducted to accompany the experimental data. The seven pure fluids and methanol-water mixtures used in the experiments were simulated at three different mass velocities and five different heat fluxes; one flux for low flow, two fluxes each for medium and high flows. A simplified geometry of the micro-channel test section was used in the simulation to reduce computation complexity. Using the same dimensions as in the experimental setup, a computational domain of a half channel/half wall running the entire 4 cm flow length was simulated. The solid portion of the heat sink was extended to the 3rd row of thermocouples (j=3). For clarity, Figure 4.2 shows the arrangement of thermocouples; each temperature measurement is named according to position in the form T_{ij} where $i = 1 - 4$ from inlet to outlet and $j = 1 - 3$ from top to bottom.

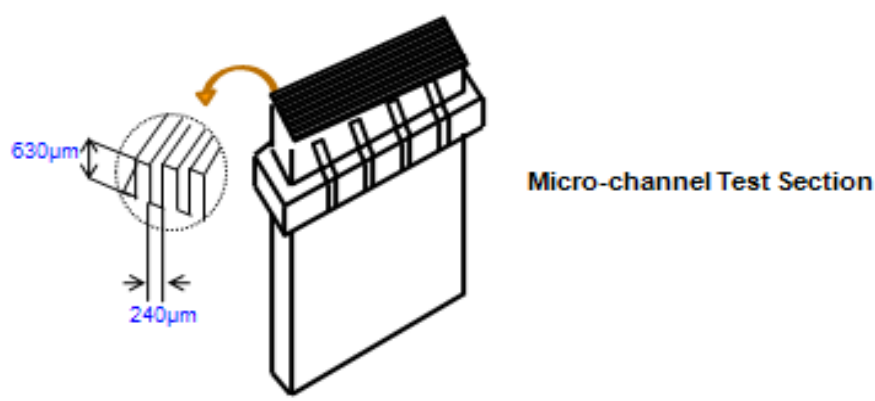

Figure 4.1: Test Section Schematic

Micro-Channel Array			
T_{11}	T_{21}	T_{31}	T_{41}
T_{12}	T_{22}	T_{32}	T_{42}
T_{13}	T_{33}	T_{33}	T_{43}
Heat Source			

Figure 4.2: Thermocouple Array

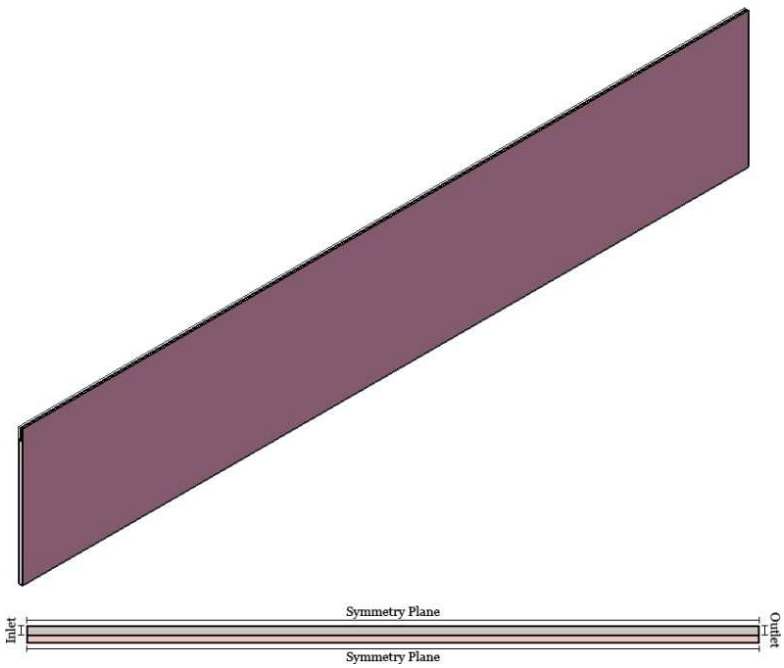

Figure 4.3: Computational Domain Used in Numerical Simulation

The simplified domain used of the following motion boundary conditions: no-slip wall, inlet, outlet and symmetry. The inlet consists of a unidirectional, constant velocity, constant temperature flow field of specifiable magnitude and temperature. The outlet consist of a constant zero pressure condition. The thermal boundary conditions used were adiabatic, symmetry and prescribed temperature. This temperature boundary condition, applied at the bottom of the simulated copper block, utilized a second order polynomial fit to the four experimental thermocouple readings ($T_{13} - T_{43}$). All other surfaces besides the fluid/solid interface were considered adiabatic. Additionally, two simplifying assumptions were made, steady and laminar flow.

The governing equations were solved using a finite-volume approach using the commercial software STAR-CCM+ ver. 6.06.011 by CD-Adapco. A second order upwind differencing scheme was used to discretize and solve the governing equations. The properties (ρ, Cp, k, μ) of the mixtures and pure fluids were modeled as functions of temperature using the correlations discussed earlier. The solution was considered to be converged when all residuals fell below 10^{-5} (relative) for continuity, momentum and energy.

The computational mesh used in the simulations was generated using STAR-CCM+'s built in polyhedral mesher with surface remeshing and a prism layer mesher for edge refinement. Three meshes were tested for independence: a 330k cell coarse, 450k cell medium, and 580k cell fine mesh. The difference between the medium and fine meshes was less than 1% and thus the medium mesh was utilized in this study. The medium mesh utilized a 35 μm base fluid cell size and a 250 μm base solid cell size. Figure 4.4 presents a portion of the mesh showing the prism layer refinement along the no-slip walls.

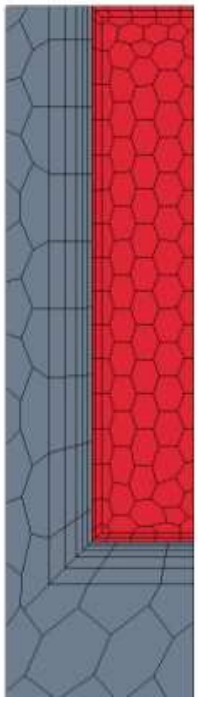

Figure 4.4: A Section of the Numerical Mesh Showing Prism Layer Refinement

4.2 Results

4.2.1 Experimental Results

The following figures present the readings obtained from thermocouples located inside the heat sink. Each figure shows both the vertical and stream-wise temperature distribution within the heat sink as a function of input heat flux for a flow rate of G = 352 kg/m^{2}s. Figure 4.5(a) shows the readings from the three vertical thermocouples in the 3rd column. It can be seen that the heat sink temperatures increase with increasing heat flux. For a given heat flux, temperature decreases from bottom to top inside the heat sink. The vertical temperature gradient increases with increasing heat flux. Figure 4.5(b) shows the stream-wise temperatures distribution along the second thermocouple row. The heat sink temperatures again increase with increasing heat flux. For a specified heat flux, temperature increases in the stream-wise direction. The temperature gradient in the stream-wise direction also increases with increasing heat flux.

Figures 4.6 - 4.8 show the readings from the same thermocouples for 36% methanol molar fraction mixture, 63% methanol molar fraction mixture, and pure methanol respectively at similar mass velocity. The general parametric trends are the same for all of the following figures. However, for a similar heat sink temperature level, the corresponding input heat flux level decreases with increasing methanol concentration. This could be attributed to inferior thermodynamic properties of methanol as compared to those of water.

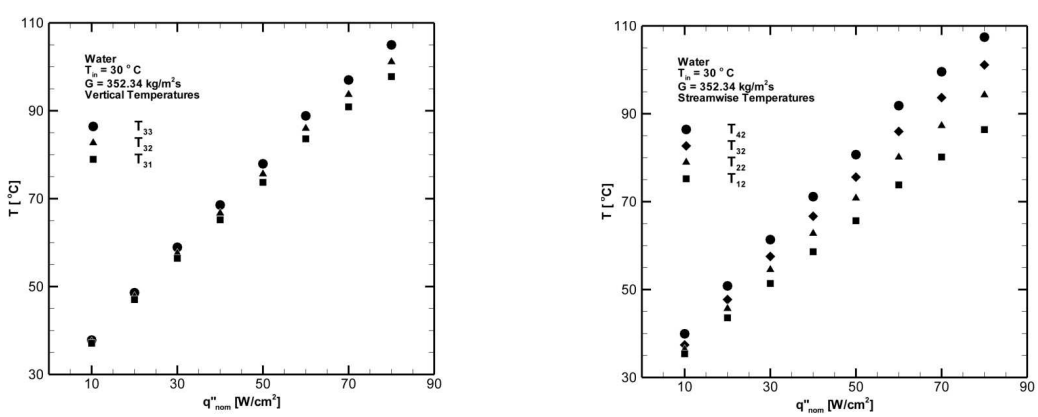

(a) (b)

Figure 4.5: Temperature Distribution in the Heat Sink for Pure Water:
(a) Vertical and (b) Stream-Wise

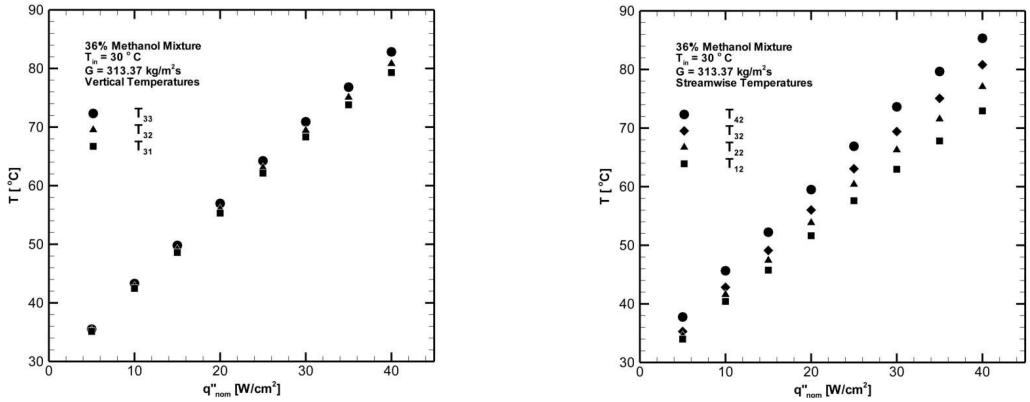

(a) (b)

Figure 4.6: Temperature Distribution in the Heat Sink for 36% Methanol Mixture: (a) Vertical and (b) Stream-Wise

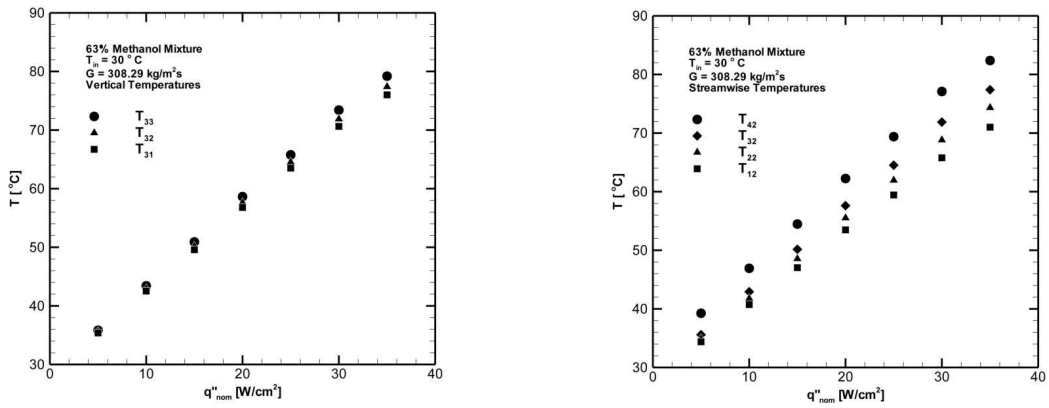

(a) (b)

Figure 4.7: Temperature Distribution in the Heat Sink for 63% Methanol Mixture: (a) Vertical and (b) Stream-Wise

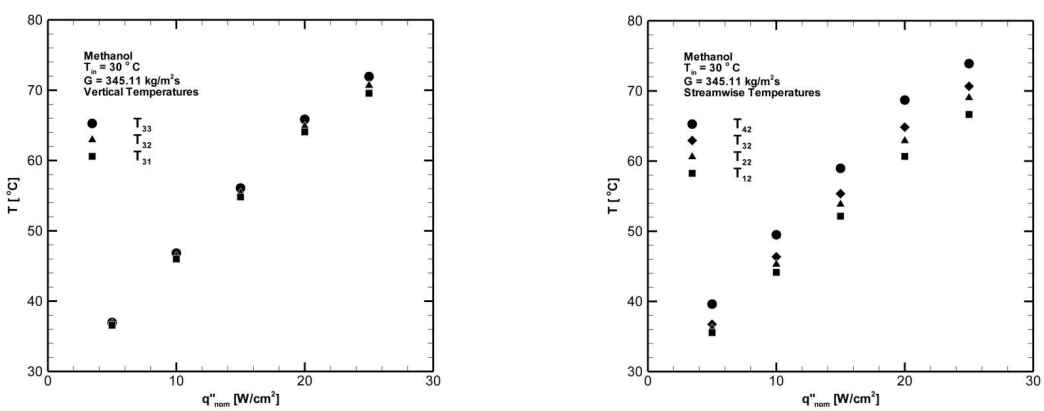

(a) (b)

Figure 4.8: Temperature Distribution in the Heat Sink for Pure Methanol: (a) Vertical and (b) Stream-Wise

4.2.2 Numerical Results

Figure 4.9 (a)-(d) compares the numerical predictions of the heat sink temperature to the experimental data for water at 50 W/cm^2, 36% methanol at 20 W/cm^2, 63% methanol at 20 W/cm^2, and pure methanol at 15 W/cm^2, respectively. A total of 35 cases were simulated numerically and the results are similar to the 4 cases presented in Figure 4.9. The good agreement between the experimental data and numerical predictions validate the present numerical model at simulating single-phase heat transfer of methanol-water mixtures in micro-channels.

In Figure 4.9 (b)-(d), the two thermocouple readings T_{21} and T_{41} do not follow the trend predicted by the numerical simulation nor follow the expected experimental values at higher methanol concentrations. This is thought to be the result of thermocouple deterioration as the deviance appears greater for the tests performed last. Experiments started with pure water and gradually increased in methanol concentration until pure methanol was tested. Towards the end of the series of experiments, it was noticed that the two thermocouples had begun to malfunction. Thus the thermocouple readings of T_{21} and T_{41} are regarded as unreliable and, although shown in Figure 4.9, are omitted in all calculations for this study.

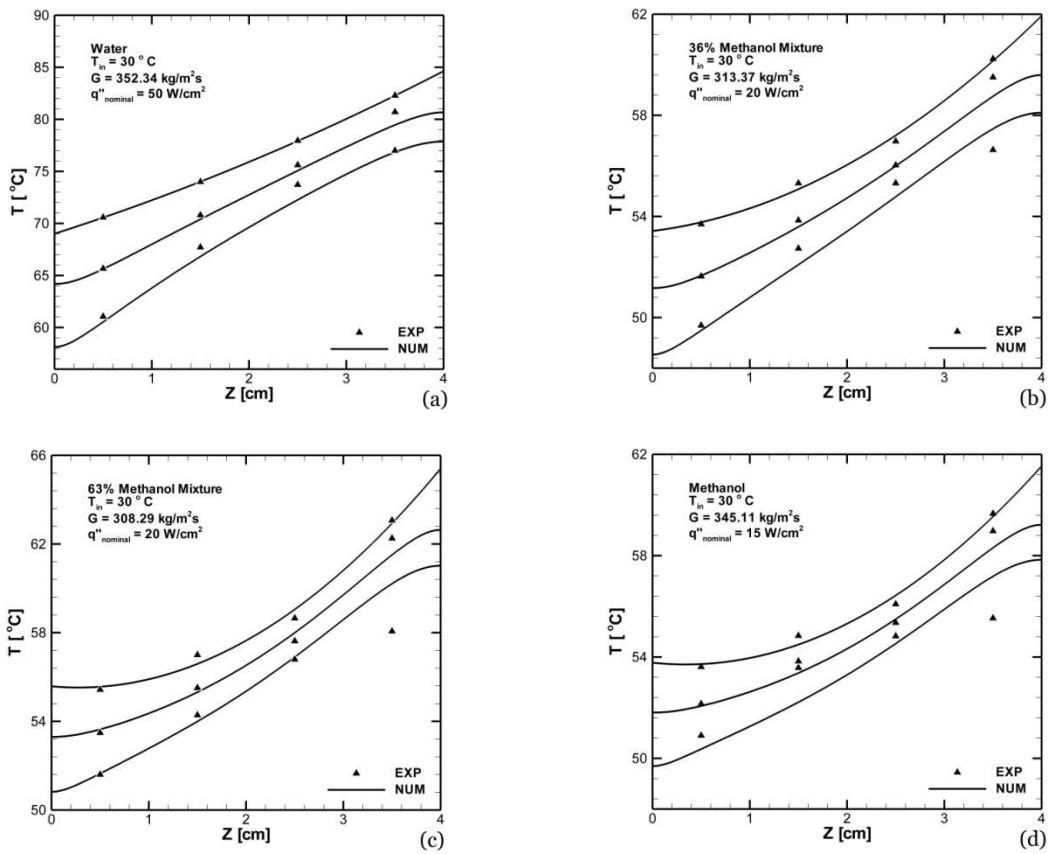

Figure 4.9: Comparison of Experimental Data and Numerical Predictions for Temperature Distribution in Stream-Wise Direction: (a) Pure Water, (b) 36% Methanol Mixture, (c) 63% Percent Methanol Mixture, and (d) Pure Methanol

In the above figure, the inlet is at z = 0cm and the outlet is at z = 4cm. The highest temperature profile belongs to the 3rd, or bottom, row of thermocouples which are closest to the heat source; the lowest temperature profile belongs to the 1st, or top, row of thermocouples which are closest to the working fluid. A 2nd order polynomial is fitted to the 3rd row of thermocouples as a Dirichlet boundary condition for numerical simulation; due to this fact, the temperature profile does not exhibit the same adiabatic, or zero slope, behavior observed for the temperature profiles of rows 1 and 2.

Chapter 5: Conclusions

In this study, experimental study and numerical simulations were conducted to examine single-phase heat transfer characteristics of methanol-water mixtures in micro-channels. Experimental results indicate that cooling performance of the mixtures decreases with increasing methanol concentration due to inferior thermodynamic properties of methanol as compared to those of water. New property subroutines for methanol-water mixtures were developed to increase the accuracy of numerical simulations; these subroutines are in good agreement with available empirical property values. The agreement between the numerical and experimental temperature profiles is good with an overall MAE for all 35 simulations of 0.87%, which indicates that numerical simulations can accurately predict experimental behavior of methanol-water mixtures in micro-channels.

Property subroutines were also developed for ethanol-water mixtures. There is a good agreement between the developed correlations and the source material. While pure property values are very mature and readily available, there is still a lack of reliable information regarding vapor phase mixture viscosity and thermal conductivity.

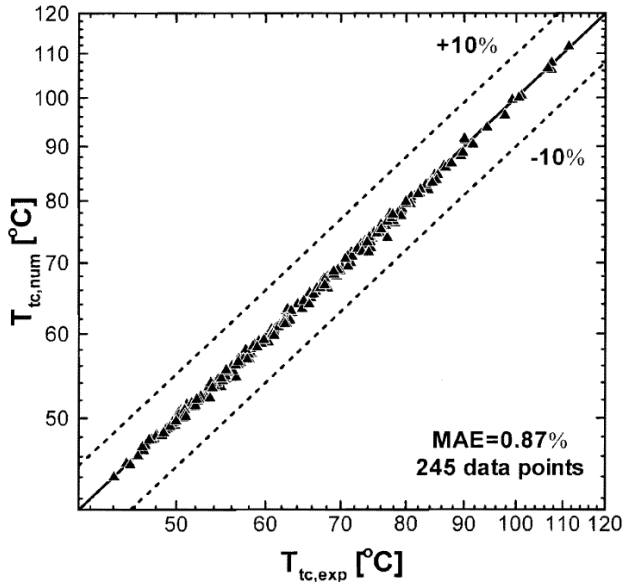

Figure 5.1: Experimental Versus Numerical Data Points

Appendix

Appendix A: Thermo-Physical Properties of Water

This appendix presents the equations for the various thermo-physical properties of water. Saturation temperature was given as a function of pressure by the form:

$$T_{sat} = C_1 + \frac{C_2}{ln(10^{-6} p) + C_3} \tag{A1}$$

where the constants are given in Table A. The equations for saturation temperature, saturated liquid density, saturated vapor density, saturated vapor viscosity, saturated liquid entropy, saturated vapor entropy, saturated liquid enthalpy, saturated vapor enthalpy, saturated liquid specific heat, saturated liquid viscosity, saturated liquid thermal conductivity were given as a function of temperature by the equations of the form:

$$h = C_1 + C_2 T_r^{1/3} + C_3 T_r^{5/6} + C_4 T_r^{7/8} + \sum_{n=1}^{7} C_{5,n} T_r^n \tag{A2}$$

The surface tension was given as a function of temperature by the equations of the form:

$$F = C_1 T_r^{C_2} (1 + C_3 T_r) \tag{A3}$$

where η is a property ratio given in Table A, the reduced temperature is:

$$T_r = \frac{T_{cr} - T}{T_{cr}} \tag{A4}$$

where T_{cr} = 374°C.

New routines for saturated vapor specific heat and saturated vapor thermal conductivity were introduced previously and are restated here for convenience.

Table 2.1: Polynomial Curve Fit Coefficients for Vapor Phase Water

	$f(T)=a1*T^4+a2*T^3+a3*T^2+a4*T+a5$				
$c_{pg}(T)$	a1	a2	a3	a4	a5
T<65	3.987×10^{-7}	4.058×10^{-5}	1.084×10^{-3}	1.047	1.884×10^{3}
T≥65	-2.130×10^{-7}	2.248×10^{-4}	-1.555×10^{-2}	1.213	1.911×10^{3}
$k_g(T)$					
T<65	2.964×10^{-12}	-2.450×10^{-10}	2.724×10^{-7}	5.253×10^{-5}	1.707×10^{-2}
T≥65	7.730×10^{-12}	-1.879×10^{-10}	3.820×10^{-7}	3.712×10^{-5}	1.768×10^{-2}

Table A.1: Thermo-Physical Properties of Saturated Water

Property	η	Range of Validity	Constants
T_{sat} [A.1]		$0.000611 \le p < 12.33$ Mpa $12.33 \le p \le 22.1$ Mpa	$C_1=4.2676$ $C_2=-3.8927\times10^3$ $C_3=-9.48654$ $C_1=-3.87592\times10^2$ $C_2=-1.25875\times10^4$ $C_3=-1.52578\times10$
ρ_f [A.1]	$\eta=\rho_{cr}/\rho_f$ $\rho_{cr}=317$ kg/m^3	$0 \le T \le 367$ °C	$C_1=1$ $C_2=-1.9153882$ $C_3=1.2015186\times10$ $C_4=-7.8464025$ $C_{5,1}=-3.888614$ $C_{5,2}=2.0582238$ $C_{5,3}=-2.0829991$ $C_{5,4}=8.2180004\times10^{-1}$ $C_{5,5}=4.7549742\times10^{-1}$ $C_{5,6}=0$ $C_{5,7}=0$
ρ_g [A.1]	$\eta=p_{sat}\rho_{cr}/p_{cr}\rho_g$ $\rho_{cr}=317$ kg/m^3 $p_{cr}=22.1$ Mpa	$0 \le T \le 367$ °C	$C_1=1$ $C_2=1.6351057$ $C_3=5.2584599\times10$ $C_4=-4.4694653\times10$ $C_{5,1}=-8.9751114$ $C_{5,2}=-4.384553\times10$ $C_{5,3}=-1.9179576\times10$ $C_{5,4}=3.6765319\times10$ $C_{5,5}=-1.9462437\times10$ $C_{5,6}=0$ $C_{5,7}=0$

h_f [A.1]	$\eta=h_f/h_{cr}$ h_{cr}=2099 kJ/kg	$0 \le T < 27\ ^oC$	$C_1=0$ $C_2=0$ $C_3=0$ $C_4=0$ $C_{5,1}=6.24698837\times10^2$ $C_{5,2}=-2.34385369\times10^3$ $C_{5,3}=-9.50812101\times10^3$ $C_{5,4}=7.16287928\times10^4$ $C_{5,5}=-1.63535221\times10^5$ $C_{5,6}=1.66531093\times10^5$ $C_{5,7}=-6.47854585\times10^4$
		$27 \le T < 327\ ^oC$	$C_1=8.839230108\times10^{-1}$ $C_2=0$ $C_3=0$ $C_4=0$ $C_{5,1}=-2.67172935$ $C_{5,2}=6.22640035$ $C_{5,3}=-1.31789573\times10$ $C_{5,4}=-1.91322436$ $C_{5,5}=6.87937653\times10$ $C_{5,6}=-1.24819906\times10^2$ $C_{5,7}=7.21435404\times10$
		$327 \le T \le 374\ ^oC$	$C_1=1$ $C_2=-4.41057805\times10^{-1}$ $C_3=-5.52255517$ $C_4=6.43994847$ $C_{5,1}=-1.64578795$ $C_{5,2}=-1.30574143$ $C_{5,3}=0$ $C_{5,4}=0$ $C_{5,5}=0$ $C_{5,6}=0$ $C_{5,7}=0$
h_{fg} [A.1]	$\eta=h_{fg}/h_{fg,tp}$ $h_{fg,tp}$=2.5 kJ/kg	$0 \le T \le 374\ ^oC$	$C_1=0$ $C_2=7.79221\times10^{-1}$ $C_3=4.62668$ $C_4=-1.07931$ $C_{5,1}=-3.87446$ $C_{5,2}=2.94553$ $C_{5,3}=-8.06395$ $C_{5,4}=1.15633\times10$ $C_{5,5}=-6.02884$ $C_{5,6}=0$ $C_{5,7}=0$

c_{pf} [A.2]	$\eta = c_{pf} / c_{pf,tp}$ $c_{pf,tp}$= 4229 $kJkg^{-1}K^{-1}$	$0 \leq T < 16.5\ ^{o}C$	C_1=-1.32167774×10^2 C_2=0 C_3=0 C_4=0 $C_{5,1}$=7.187539242×10^2 $C_{5,2}$=-1.293389294×10^3 $C_{5,3}$=7.759108594×10^2 $C_{5,4}$=0 $C_{5,5}$=0 $C_{5,6}$=0 $C_{5,7}$=0
		$16.5 \leq T < 61\ ^{o}C$	C_1=4183/ $c_{pf,tp}$ C_2= 0 C_3=0 C_4=0 $C_{5,1}$=0 $C_{5,2}$=0 $C_{5,3}$=0 $C_{5,4}$=0 $C_{5,5}$=0 $C_{5,6}$=0 $C_{5,7}$=0
		$61 \leq T < 367\ ^{o}C$	C_1=8.155995578×10 C_2=-8.859959196×10^2 C_3=1.050250972×10^5 C_4=-1.442971474×10^5 $C_{5,1}$=4.192929369×10^4 $C_{5,2}$=-4.025751358×10^3 $C_{5,3}$=6.09997762×10^3 $C_{5,4}$=-1.020112319×10^4 $C_{5,5}$=1.309194799×10^4 $C_{5,6}$=-1.05497178×10^4 $C_{5,7}$=3.898938483×10^3
μ_f [A.4]	$\eta = \log(\mu_f / \mu_{f,tp})$ $\mu_{f,tp}$= 1791×10^{-6} Ns/m^2	$0 \leq T < 374\ ^{o}C$	C_1=-1.66203042 C_2=2.62821734×10^{-1} C_3=2.491805408×10^2 C_4=-3.776335187×10^2 $C_{5,1}$=1.443250321×10^2 $C_{5,2}$=-6.266348045×10 $C_{5,3}$=2.436111833×10^2 $C_{5,4}$= -7.753578652×10^2 $C_{5,5}$=1.634865202×10^3 $C_{5,6}$=-1.932335223×10^3 $C_{5,7}$=9.738731615×10^2

μ_g [A.4]	$\eta=\mu_f/\ \mu_{g,tp}$ $\mu_{g,tp}=$ 9.22×10^{-6} Ns/m^2	$0 \leq T < 374\ ^oC$	$C_1=4.229934564$ $C_2=-7.770295047$ $C_3=5.831494678\times10^2$ $C_4=-8.432248947\times10^2$ $C_{5,1}=2.912530753\times10^2$ $C_{5,2}=-8.864011148\times10$ $C_{5,3}=2.288934411\times10^2$ $C_{5,4}=-5.249549317\times10^2$ $C_{5,5}=8.155507497\times10^2$ $C_{5,6}=-7.296627070\times10^2$ $C_{5,7}=2.850617583\times10^2$
k_f [A.4]	$\eta=k_f/\ k_{f,tp}$ $k_{f,tp}=0.561$ $Wm^{-1}K^{-1}$	$0 \leq T \leq 372\ ^oC$	$C_1=3.936182706$ $C_2=-5.07394162\times10$ $C_3=9.05494387\times10^3$ $C_4=-1.280730752\times10^4$ $C_{5,1}=4.046852934\times10^3$ $C_{5,2}=-6.386971807\times10^3$ $C_{5,3}=1.287531215\times10^3$ $C_{5,4}=-2.6346998\times10^3$ $C_{5,5}=3.976737235\times10^3$ $C_{5,6}=-3.649471543\times10^3$ $C_{5,7}=1.475458591\times10^3$
σ_f [A.5]		$0 \leq T < 374\ ^oC$	$C_1=0.2358$ $C_2=1.256$ $C_3=-0.625$

[A.1]Equations obtained from Irvine and Liley (1984).
[A.2]Equations developed using data tabulated in Grigull *et al*. (1990).
[A.3]Equations developed using data tabulated in Ierardi *et al*. (1999).
[A.4]Equations developed using data tabulated in Haar *et al*. (1984).
[A.5]Equations obtained from Haar *et al*. (1984).

Bibliography

[1] D. B. Tuckerman and R. F. Pease, "High Performance Heat Sinking for VLSI," IEEE Electronic Devices Letters, EDL-2(5), pp.126-129, 1981.

[2] R. J. Phillips, "Micro-Channel Heat Sinks," Advances in Thermal Modelling of Electronic Components, A. Bar-Cohen, and A.D. Kraus, eds., ASME Press, New York, 2, pp. 109-184, 1990.

[3] K. Kawano, K. Minakami, H. Iwasaki and M. Ishizuka, "Micro Channel Heat Exchanger for Cooling Electrical Equipment," Proceedings of the ASME Heat Transfer Division, ASME HTD-361-3/PID-3, pp. 173-180, 1998.

[4] T. M. Harms, M. J. Kazmierczak and F. M. Cerner, "Developing Convective Heat Transfer in Deep Rectangular Microchannels," International Journal of Heat and Fluid Flow, 20(2), pp. 149-157, 1999.

[5] W. Qu and I. Mudawar, "Experimental and Numerical Study of Pressure Drop and Heat Transfer in a Single-Phase Micro-Channel Heat Sink," International Journal of Heat and Mass Transfer, 45(12), pp. 2549-2565, 2002.

[6] P. S. Lee and S. V. Garimella, "Inversitgation of Heat Transfer in Rectangular Microchannels," International Journal of Heat and Mass Transfer, 48(9), pp. 1688-1704, 2005.

[7] G. W. Warrier, V. K. Dhir and L. A. Momoda, "Heat Transfer and Pressure Drop in Narrow Rectangular Channel," *Exp. Therm. Fluid Sci.,* no. 26, pp. 53-64, 2002.

[8] H. J. Lee and S. Y. Lee, "Heat Transfer Correlation for Boiling Flows in Small Rectangular Horizontal Channels with Low Aspect Ratios," *Int. J. Multiphase Flow,* no. 22, pp. 2043-2062, 2001.

[9] T. N. Tran and D. M. Wambsganss, "Small Circular and Rectangular Channel Boiling with Two Refrigerants," *Int. J. Multiphase Flow,* no. 22, pp. 485-498, 1996.

[10] K. Mishima and T. Hibiki, "Some Characteristics of Air-Water Two-Phase Flow in Small Diameter Vertical Tubes," *Int. J. Multiphase Flow,* no. 45, pp. 39-48, 1996.

[11] D. S. Jung, M. McLinden, R. Radermacher and D. Didion, "Horizontal Flow Boiling Heat Transfer Experiments with Mixture of R22/R114," *Int. J. Heat Mass Transfer,* no. 32, pp. 131-145, 1989.

[12] D. S. Jung, M. McLinden, R. Radermacher and D. Didion, "A Study of Flow Boiling Heat Transfer Experiments with Refrigerant Mixtures," *Int. J. Heat Mass Transfer,* no. 32, pp. 1751-1764, 1989.

[13] G. P. Celata, M. Cumo and T. Setaro, "A Review of Pool and Forced Convective Boiling of Binary Mixtures," *Experimental Thermal and Fluid Science,* no. 32, pp. 367-381, 1994.

[14] E. W. Lemmon, M. L. Huber and M. O. McLinden, "NIST Standard Reference Database 23: Reference Fluid Thermodynamic and Transport Properties - REFPROP, Version 9.0," National Institute of Standards and Technology, Standard Reference Data Program, Gaithersburg, 2010.

[15] E. W. Lemmon, "Answers to Frequently Asked Questions," 2012. [Online]. Available: http://www.boulder.nist.gov/div838/theory/refprop/Frequently_asked_questions.htm.

[16] E. W. Lemmon and R. T. Jacobsen, "A New Functional Form and New Fitting Techniques for Equations of State with Application to Pentafluoroethane (HFC-125)," NIST, Boulder, CO, 2005.

[17] C. K. Kwok, "Flow Boiling Heat Transfer to Methanol-Water Mixture in Micro-Channels," MS Thesis, University of Hawaiʻi, Mānoa: United States, 2010.

[18] W. Wagner and A. Pruss, "The IAPWS Formulation 1995 for the Thermodynamic Properties of Ordinary Water Substance for General and Scientific Use," *J. Phys. Chem. Ref. Data,* vol. 31, no. 2, pp. 387-535, 2002.

[19] K. M. de Reuck and R. J. B. Craven, Methanol, International Thermodynamic Tables of the Fluid State - 12, London: IUPAC, Blackwell Scientific Publications, 1993.

[20] D. W. Green and R. H. Perry, "Perry's Chemical Engineers' Handbook," McGraw-Hill, New York, NY, 2008.

[21] J. Li and P. W. Carr, "Accuracy of Empirical Correlations for Estimating Diffusion Coefficients in Aqueous Organic Mixtures," *Analytical Chemistry,* vol. 69, pp. 2530-2536, 1997.

[22] J. Billen, K. Broeckhoven, A. Liekens, K. Choikhet, G. Rozing and G. Desmet, "Influence of Pressure and Temperature on the Physico-Chemical Properties of Mobile Phase Mixtures Commonly Used in High-Performance Liquid Chromatography," *Journal of Chromatography A,* vol. 1210, pp. 30-44, 2008.

[23] H. Colin, J. C. Diez-Masa, T. Czaykowska, I. Miedziak and G. J. Guiochon, "The role of the temperature in reversed-phase high-performance liquid chromatography using pyrocarbon-containing adsorbents," *Journal of Chromatography,* vol. 167, pp. 41-65, 1978.

[24] C. F. Spencer and R. P. Danner, *J. Chem. Eng. Data,* vol. 17, p. 236, 1972.

[25] C. C. Li, *Can. J. Chem. Eng.,* vol. 19, p. 709, 1971.

[26] R. W. Falta, K. Pruess, F. Stefan and A. Battistelli, "T2VOC User's Guide," Lawrence Berkeley Laboratory, Berkeley, CA, 1995.

[27] B. E. Poling, J. M. Prausnitz and J. P. O'Connell, "The Properties of Gases and Liquids," McGraw-Hill, New York, 2001.

[28] R. B. Bird, W. E. Stewart and E. N. Lightfoot, Transport Phenomenon, New York: Wiley, 1960.

[29] E. A. Mason and S. C. Saxena, *Phys. Fluids,* vol. 1, p. 361, 1958.

[30] H. E. Dillon and S. G. Penoncello, "A Fundamental Equation for Calculation of the Thermodynamic Properties of Ethanol," *Int. J. Thermophys.,* vol. 25, no. 2, pp. 321-335, 2004.

[31] Y. Tanaka, T. Yamamoto, Y. Satomi, H. Kuboto and T. Makita, "Specific Volume and Visocisity of Ethanol-Water Mixtures Under High Pressure," *The Review of Physical Chemistry of Japan,* vol. 47, no. 1, pp. 12-24, 1977.